Journal of Molecular Liquids 377 (2023) 121322

Contents lists available at ScienceDirect

Journal of Molecular Liquids

journal homepage: www.elsevier.com/locate/molliq

Hydrophobic Deep eutectic Solvents based on cineole and organic acids

Jose L. Trenzado [a], Cristina Benito [b], Mert Atilhan [c,*], Santiago Aparicio [b,*]

[a] Department of Physics, University of Las Palmas de Gran Canaria, 35017 Las Palmas G.C., Spain
[b] Department of Chemistry, University of Burgos, 09001 Burgos, Spain
[c] Department of Chemical and Paper Engineering, Western Michigan University, Kalamazoo, MI, USA

ARTICLE INFO

Article history:
Received 19 October 2022
Revised 12 January 2023
Accepted 24 January 2023
Available online 27 January 2023

Keywords:
Deep Eutectic Solvents
Hydrophobic
Natural
Thermophysics
COSMO
Molecular Dynamics

ABSTRACT

The hydrophobic Natural Deep Eutectic Solvent formed by the combination of cineole and decanoic acid (capric acid) was studied using a combined experimental and computational approach. Experimental study was carried considering relevant physicochemical properties as density, viscosity, refraction index and thermal conductivity as a function of temperature, as well as Raman spectra for 785 nm excitation wavelength. Thermophysical properties measured showed a low -viscous low-dense fluid, which is of great relevance for its technological application, as well as the Raman spectra confirmed the formation of hydrogen bonding. The analysis of nanoscopic properties and structuring was carried out using theoretical method as the Density Functional Theory (BP86/def2-TZVP plus Grimme's D3 theoretical level) and classical Molecular Dynamics simulation (using AMOEBA polarizable force field). Molecular modelling studies using quantum chemistry and classical molecular dynamics methods allowed a nanoscopic characterization of the fluid as well as of its intermolecular forces (hydrogen bonding). Phase equilibria were predicted using COSMO method considered solid–liquid (melting behavior) and vapor – liquid (evaporation), as well as excess properties. The COSMO results showed a low volatile, wide liquid range fluid, characterized by non-ideality because of the formation of hydrogen bonding. Likewise, the interaction of the considered material with POPC lipid was studied using COSMOperm method to analyze its behavior at lipid bilayers as models of cell membranes for the consideration of its possible toxicological effects, showing how the considered molecules are able to penetrate and disrupt the model membranes because of the lipophilic nature of the considered molecules.

1. Introduction

Deep Eutectic Solvents (DESs) [1,2] are a class of fluids formed by the combination of two or more suitable compounds, which upon mixing at a certain mole ratio leads to a system (eutectic mixture) with melting point remarkably lower than the ones for the corresponding components of the mixture [3]. This melting point depression use to lead to systems being liquid at ambient temperature, which have been considered as suitable fluids for possible applications in a plethora of technologies, in particular for a sustainable chemistry framework [4]. Therefore, applications proposed consider water treatment [5], gas purification and separation (with particular interest on CO_2 capture) [6], metal processing [7], synthesis and catalysis [8], agrifood sector [9], pharmacological [10], polymer science [11] and many others. The possibility of controlling the properties of the formed DES by selecting suitable components led to a large number of possible DES which properties can be designed according to the required technological application (task – specific fluids) [12]. DES can be initially classified in five different categories depending of the involved components [1], with most of the available studies and applications developed around the so-called type *iii* DES, which are usually formed by a salt and an organic molecule. In these type of DES, the combination of an hydrogen bond donor (HBD) and an hydrogen bond acceptor (HBA) leads to strong intermolecular hydrogen bonding [13,14], which is on the root of the DES formation and on the melting point decrease in comparison with DES components [15,16]. A recently proposed type of DESs is the so-called type *v* DES [17], which are usually formed by the combination of non-ionic HBAs and HBDs. Another relevant DES classification stands on the origin of the involved DES components, thus, the so-called natural DES (NADES) have been proposed as formed by HBAs and HBDs with natural origin [18], thus being low cost, highly biodegradable and low toxic, therefore being the most sustainable type of DES. The well-known effect of water on DES properties have led to the distinction between hydrophobic and

* Corresponding authors.
E-mail addresses: mert.atilhan@wmich.edu (M. Atilhan), sapar@ubu.es (S. Aparicio).

https://doi.org/10.1016/j.molliq.2023.121322
0167-7322/

hydrophilic DES/NADES with the first ones having remarkable advantages such as their usually low viscosity [19], which improves their performance for relevant industrial operations such as those involving heat or mass transfer, lower density when compared with water and applicability in a large collection of technologies [20].

The interest on hydrophobic DES has increased these last years, both for those of type iii [21] and type v [22] categories. These fluids have been proposed in application in food sector [23], water treatment [24], Volatile Organic Compounds elimination [25], CO_2 capture [26], extraction of valuable compounds [27], or in pharmacological applications [28]. The main characteristic of hydrophobic DES stand on the low-density, low-viscosity for those belonging to type v, with fluids such as those formed by the combination of menthol – decanoic acid or thymol – decanoic acid showing 0.896 and 0.918 g cm^{-3}, for density respectively, or 12.71 or 11.13 mPa s, for viscosity respectively, at 298.15 K [29]. Likewise, in spite of their hydrophobic nature, it has been probed that small water amounts (e.g. obtained from atmospheric water absorption) have remarkable effects on the fluid properties, increasing density and decreasing viscosity, e.g. for type iii Tetrabutylammonium chloride – decanoic acid 1: 2 DES viscosity decreases from 425 mPa s for neat DES to 80 mPa s for DES with 2.5 wt% water content [30]. Regarding the toxicity, safety and possible environmental impact of hydrophobic DES, studies are still scarce. Nevertheless, available studies have probed that common components of hydrophobic DES show moderate toxicity [31] and even some of these DES have been applied for therapeutic applications [28,32]. Additionally, sustainability of hydrophobic DES has been probed, e.g. menthol – fatty acids have been applied for water treatment showing a fully circular approach [33]. Therefore, the formation of natural and hydrophobic DES [34] combines most of the relevant features favoring technical application of DESs as well as being suitable fluids for being scaled up to several relevant technologies.

The objective of developing hydrophobic NADES being suitable for different technologies is considered in this work through the analysis of the properties of NADES formed by the combination of a monoterpenoid (cineole, CIN), acting as HBA, and a saturated fatty acid (decanoic acid, C10), acting as HBD, Fig. 1a. The properties of monoterpenoid – based NADES have been studied in the literature [35], being a suitable platform for developing sustainable solvents. CIN is a natural compound, which can be obtained from vegetal sources such as eucalyptus leaves or several plant essential oils [36] and it also can be biosynthesized [37], being non-toxic, the trading price is in the 10–20 USD per kg although it can be produced at relatively low-price (lower than 5 USD per kg [38]). C10 is also a natural compound being obtained from sources such as palm or coconut oil [39] also at very low cost (roughly around 2 USD per kg). The considered CIN: C10 (1: 1), Fig. 1, was selected as prototypical monoterpenoid + fatty acid hydrophobic NADES, which properties are analyzed using a combined experimental and theoretical approach considering both micro and macroscopic viewpoints. Relevant physicochemical properties required for industrial design and applications are measured as a function of temperature. The suitability of COSMO methods for the prediction of DES / NADES properties has been confirmed in the literature [40,41], and thus they were applied for the prediction of phase equilibria as well as for the analysis of interfacial properties (at vacuum and water interfaces) and for the interaction with model lipid bilayers to quantify the behavior of the considered NADES at cell membranes [42], as a possible Molecular Initiating Event (MIE) into an Adverse Outcome Pathway (AOP) for possible toxicity effects [43,44]. Considering the advances on the description, properties prediction and nanoscopic structuring analysis of DES / NADES via molecular modelling methods [45–47], CIN: C10 (1: 1) hydrophobic NADES was studied using quantum chemistry methods (Density Functional Theory, DFT) and classical Molecular Dynamics (MD) simulations for the analysis and quantification of intermolecular forces (hydrogen bonding) and liquid structuring in terms of aggregation, energy of interactions, and dynamic properties. The reported results allowed a multiscale characterization of the considered hydrophobic NADES.

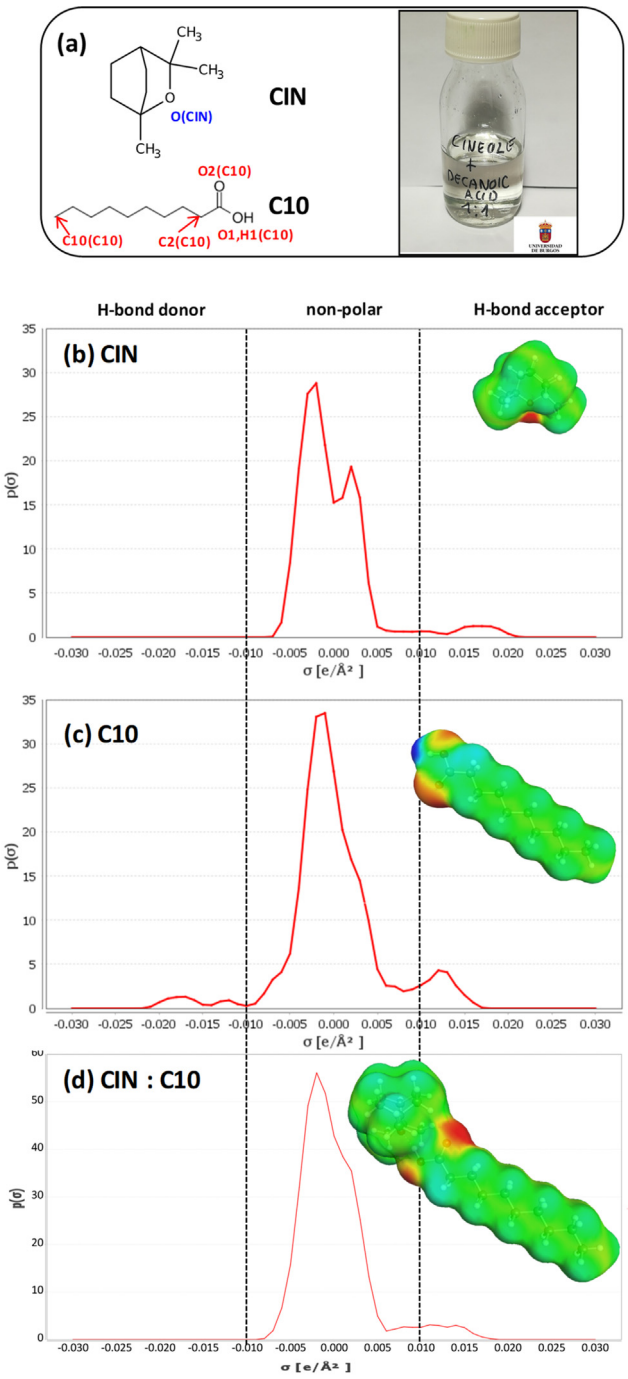

Fig. 1. (a) Molecules used for the DES development in CIN: C10 1: 1 composition as well as sample of the considered DES at 293 K. Panels b to d show COSMO profiles (indicating regions for different intermolecular interaction mechanism) as well as molecular surfaces indicating regions with high (red) and low (blue) electron density. Relevant atom labelling is indicated in panel a. (For interpretation of the references to colour in this figure legend, the reader is referred to the web version of this article.)

2. Methods

2.1. Chemicals

The origin and purity of pure CIN and C10 used for the DES preparation are reported in Table S1 (Supplementary Information). High purity chemicals were used and thus no further purification was carried out. The preparation of the DES (CIN: C10 1: 1 mol ratio) was done by weighing (Mettler AT261 balance, ± 1 10^{-5} g) suitable amounts and heating under stirring at 40 °C in closed vials. Liquid samples were formed and dried under vacuum using a Heidolph rotary evaporator at 40 °C. All the samples were stored in closed vessels under vacuum to avoid water sorption from atmosphere. The water content of the samples was measured using a Karl-Fischer coulometric titrator (Metrohm 831 KF coulometer, ± 0.3 %) with the samples used for the determination of the considered physicochemical properties having 0.07 wt% water content. A transparent, colorless, low viscous fluid is formed (Fig. 1a), which remain in liquid state for weeks without any sign of crystallization or turbidity at ambient temperature.

2.2. Apparatus and procedures

Melting point of the considered DES was measured by controlled cooling of a liquid sample placed in a suitable vessel, with the temperature controlled by a external liquid bath and measured with a platinum resistance thermometer (PRT, ±0.01 K). Samples under stirring were slowly cooled and the appearance of solid phase was visually observed. The ability of DES to capture water from atmospheric humidity was experimentally measured through a kinetic experiment in which a DES (15 cm^3) sample was placed in a petri dish (90 mm of diameter, 25.5 cm^2 of liquid surface exposed to air) and exposed to atmosphere (50 ± 5 % relative humidity). Samples (~0.1 g) were extracted as a function of time and the water content determined with Karl-Fischer coulometer. The experimental water content (m_w, in wt %) vs time (t) data results were fitted to the following kinetic model:

$$m_w = m_w^{\infty}(1 - exp(-kt)) \quad (1)$$

With m_{water}^{∞} being the limiting absorption value, and k the absorption rate.

The following physicochemical properties (Table S2, Supplementary Information) were measured for the considered DES: density, shear viscosity, refractive index and thermal conductivity. These properties were measured in the 293.15 to 333.15 K, except refraction index which was measured to 323 K. Thermal conductivity was measured only at 293.15 K because its variation in the 293.15 to 333.15 K range was below the uncertainty limit.

Density (ρ) was measured with a vibrating tube densimeter (Anton Paar DMA1001, uncertainty 1 10^{-4} g cm^{-3}), with Peltier control for the cell temperature (uncertainty 0.01 K). The thermal expansion coefficient, α_p, was calculated according to its thermodynamic definition:

$$\alpha_p = -\frac{1}{\rho}\left(\frac{\partial \rho}{\partial T}\right)_p = -\frac{1}{\rho}a \quad (2)$$

where a is the slope of the corresponding ρ vs temperature linear fit.

The refraction index, n_D, was measured with regard to the sodium D-line with a Leica AR600 (uncertainty 1 10^{-5}). The refractometer cell temperature was controlled through an external circulating bath (Julabo F30) and measured with a built in PRT (±0.01 K). The experimental n_D was used to calculate the molar free volume, f_m, [48], according to the following equation:

$$f_m = \frac{M}{\rho}\left(1 - \frac{n_D^2 - 1}{n_D^2 + 2}\right) \quad (3)$$

Shear viscosity (η, uncertainty 2 %) was measured with an electromagnetic piston viscometer (VINCI Tech EV1000) [49], with the temperature controlled with an external circulating bath (Julabo Presto) and measured with a PRT (±0.01 K). The viscosity vs temperature evolution was followed a non-Arrhenius behavior, and thus, it was fitted to the Vogel-Fulcher-Taman (VFT) model: $\eta = \eta_0 exp\left(\frac{B}{T-T_0}\right)$(4).

VFT fitting parameters were used for the calculation of Angell's strength (fragility measurement) parameter, D_f.

$$D_f = \frac{B}{T_0} \quad (5)$$

Thermal conductivity (σ, 5 % uncertainty) was measured with a Decagon devices KD2 Thermal analyzer (KS-1 sensor, 6 cm long, 1.3 mm diameter single needle. Sample was placed inside a temperature- controlled cell (external circulating bath Julabo F32) and measured with a PRT (±0.01 K).

Raman spectra were collected using a StellarNet-HR-TEC-785 spectrometer (4 cm^{-1} resolution) for a 785 nm laser excitation wavelength including an enhanced CCD array detector.

2.3. Density Functional Theory calculations

Density Functional Theory (DFT) calculations were carried out with Turbomole [50] software. The main objective of DFT calculations is to analyze the nature of intermolecular forces in the considered DES, in particular for the characteristics of hydrogen bonding. For this purpose, CIN: C10 dimmers and tetramers were built and geometrically optimized. All the calculations were carried out at the BP86/def2-TZVP plus Grimme's D3 [51] dispersion contribution. The optimized geometries for the considered clusters were used for the calculation of interaction energy, ΔE, as the difference between the energy of the corresponding cluster and the sum of the corresponding monomers. All the ΔE were corrected for the basis set superposition error (BSSE) using counterpoise method [52]. The main intermolecular forces were analyzed considering the Quantum Theory of Atoms in Molecule (Bader's QTAIM theory) [53] as include in MultiWFN software [54]. The QTAIM analysis of intermolecular forces was done through the properties, electron density (ρ) and Laplacian of the electron density ($\nabla^2\rho$), of bond (BCPs, type (3,-1) in QTAIM) and Ring (RCPs, type (3,-1) in QTAIM) critical points. Non-Covalent Interaction analysis (NCI [55]) and electron localization function (ELF) using Core-valence bifurcation index (CVB [56]) were used for the characterization of interactions in the optimized clusters. Likewise, Interaction Region Indicator (IRI) analysis [54] was carried out.

The COSMOtherm software [57] was used for the prediction of selected thermodynamic properties, for the analysis of interfacial behavior as well as for the interaction of the considered DES with POPC (1-palmitoyl-2-oleoyl-*sn-glycero*-3-phosphocholine) lipid molecules in model bilayers (COSMOperm) [42]. The CIN: C10 (1: 1) pair structure optimized at BP86/def2-TZVP/D3 theoretical level were used as inputs for COSMO calculations, for which single point BP86/def-TZVP were carried out.

2.4. Classical molecular dynamics simulation

MD simulations were carried out using TINKER software [58]. All simulations were carried out with AMOEBA09 polarizable forcefield [59] with forcefield type assignation as in Figure S1 (Supplementary Information). Initial cubic simulations boxes for the systems explained in Table S3 (Supplementary Information) to

mimic CIN: C10 (1: 1) DES were built using Packmol [60] program. Temperature and pressure for the systems were controlled with Nose-Hoover method [61] . The Ewald method [62] was considered for treating electrostatic interactions. MD simulations were carried out in a two-stages procedure for each pressure–temperature condition (Table S3, Supplementary Information): *i*) 1 ns equilibration in the NVT ensemble then followed by *ii*) 50 ns NPT simulations. Proper equilibration was assured through the time evolution of total potential energy, calculated physical properties (e.g. density) and through the development of fully diffusive regime by the analysis of log–log plots of mean-square displacements (*msd*) versus simulation time, leading to slopes in the 0.98–1.00. The low viscosity of the considered DES (<7.1 mPa s for the considered temperature range, Table S2, Supplementary Information) assures proper sampling of the considered liquid systems. MD trajectories visualization and analysis were carried out with TRAVIS [63] and VMD [64].

3. Results and discussion

The CIN: C10 (1: 1) hydrophobic NADES is a colorless liquid, Fig. 1a, with 282 K melting temperature. The properties of the molecules involved in the considered DES are firstly analyzed by using COSMOtherm approach through the consideration of the so-called COSMO σ-profiles [65], Fig. 1b to 1d. The properties of the isolated DES components were compared with those upon DES pair formation. The σ-profiles allow to identify non-polar, hydrogen bonding and acceptor regions in the considered molecules. The CIN molecule is characterized by high electron density region around the ether group surrounded by a large non-polar bulky region, which is showed in the σ-profiles by the large non-polar peaks and the formation of and HBA smaller peak. For C10, the high electron density region around both oxygen atoms and the low electron density in the hydroxyl hydrogen atom confirms the HBA and HBD character of the molecules as well as the large hydrophobic character as showed by the large non-polar peak in σ-profile. The formation of the DES is accompanied by the development of CIN – C10 hydrogen bonding, which results in a dimer with two electron rich areas around the oxygen atoms of C10 and large hydrophobic areas around it, and thus, this dimmer may act also as HBA with neighbor dimmers. Therefore, the CIN – C10 dimmer, which may be considered as the minimal constituent of the liquid DES structuring, is a large hydrophobic molecular moiety with HBA nature.

The COSMOtherm method was also applied for predicting relevant phase equilibria and mixing properties to understand the liquid macroscopic properties of the considered DES. Results in Fig. 2a shows the predicted isobaric (1 bar) Solid-Liquid Equilibria (SLE) for CIN + C10 mixtures as a function of mixture composition. It should be remarked that the true eutectic composition is obtained for CIN: C10 (2: 1), i.e. rich CIN DES leads to the largest melting point decrease upon comparison with those for independent components. Nevertheless, the DES formed by CIN: C10 in 1: 1 composition also has a low melting temperature being liquid at ambient conditions, and it is much more hydrophobic than the one formed by 2 CIN: 1 C10 eutectic mixture, therefore the equimolar DES was considered for this work to target a hydrophobic fluid. The COSMOtherm prediction for the melting point of the equimolar DES is only 12 K lower than the experimental value, which confirms its suitability for predicting phase equilibria of the considered DES. Vapor – liquid equilibria (VLE) were also predicted using COSMOtherm approach, Fig. 2b and 2c, showing low volatility for the considered DES. This is another advantage of considering CIN: C10 (1: 1) composition as the (2: 1) eutectic composition is more volatile. The calculated VLE indicates that no vaporization is inferred at ambient pressure up to 500.4 K, which combined with the low melting point leads to a 230.4 K liquid window, and thus showing the suitability of the considered DES as a wide temperature range solvent. The formation of CIN: C10 (1: 1) DES is produced by the mixing of the independent components, which upon hydrogen bonding formation leads to the DES, therefore the analysis of the mixing properties is relevant to characterize the thermodynamics of the DES formation. For this purpose, activity coefficients, Fig. 2d, and excess properties, Fig. 2e, were predicted also using COSMOtherm. The predicted activity coefficients show largely non-ideal behavior for CIN - C10 mixtures, with values lower than unit for both components in the whole composition range, which indicate strong CIN – DES heteroassociations in the whole mixing range. Activity coefficients at infinite dilution are 0.16 and 0.05 for CIN and C10, respectively, which indicate the hydrogen bonding ability of both DES components. At 1: 1 (equimolar) composition the activity coefficients are 0.43 and 0.64 for CIN and C10, respectively, indicating again the formation of CIN – C10 hydrogen root being on the root of DES mixture formation non-ideality. Exothermic mixing is predicted with an excess enthalpy of −6.6 kJ mol^{-1} for the formation of CIN: C10 (1: 1) DES, which agrees with the large deviations from ideality reported in Fig. 2d. Literature studies have showed endothermic processes of formation of some well-known type *iii* DES, e.g. the formation of DES involving quaternary salts such a choline chloride (ChCl): glycerol (1: 2) or ChCl: ethylene glycol (1: 2) led to excess enthalpies of 4.1, 5.4 kJ mol^{-1}, respectively [66], which are in remarkable contrast with the largely negative excess enthalpy for CIN: C10 DES. Therefore, no external heating is required for the formation of CIN: C10 (1:1) DES, which is largely relevant for the industrial application and upscaling of the considered DES both considering economical and technical aspects. Moreover, these results are in agreement with literature data on other type *v* DES, e.g. those involving flavonoids and monoterpenoids also leading to largely exothermic mixing processes [67], thus showing advantageous behavior of type *v* DES in comparison with type *iii* ones in terms of energy costs for preparation. The CIN: C10 DES formation through mixing was also analyzed considering the excess Gibbs energy, Fig. 2e, which although being negative, confirming spontaneous DES formation, is less negative than the excess enthalpy, thus indicating negative mixing entropy (-3.9 J $mol^{-1}K^{-1}$ for equimolar mixture). The negative excess entropy results from the formation of CIN – C10 heteroassociation through hydrogen bonding, although the CIN – CIN (dipolar) and the C10 – C10 (hydrogen bonding) interactions are disrupted upon DES formation (which is a factor increasing entropy) the formed heteroassociations (a factor decreasing entropy) seem to prevail resulting in the negative excess entropy, which again contrast with positive excess entropy for type *iii* DES [66]. Therefore, the reported thermodynamics analysis of the mixing process leading to CIN: C10 (1: 1) formation confirms the large trend to develop heteroassociations through hydrogen bonding as being the driving force for the DES formation.

The properties of relevant CIN: C10 (1: 1) interfaces were also analyzed considering the COSMOtherm approach. First, the properties at vacuum interface were predicted, Fig. 3a and 3b. The concentration profiles at the vacuum interface shows an enrichment of the interface with CIN molecules in comparison with bulk liquid, with C10 molecules placed in inner areas of the interface region. The predicted interface tension (IFT) is lower than for most of the DES considered in the literature. ChCl – based type *iii* DES show IFT values (usually measured at the air interface but comparable to the value reported in this work for vacuum interface) in the 40 to 70 mN m^{-1} range [68]. The IFT values are related with the strength of the hydrogen bonding, the stronger the interaction the larger the IFT. The low IFT obtained for CIN: C10 (1: 1) is justified by the structuring of the interface reported in Fig. 3a, although strong

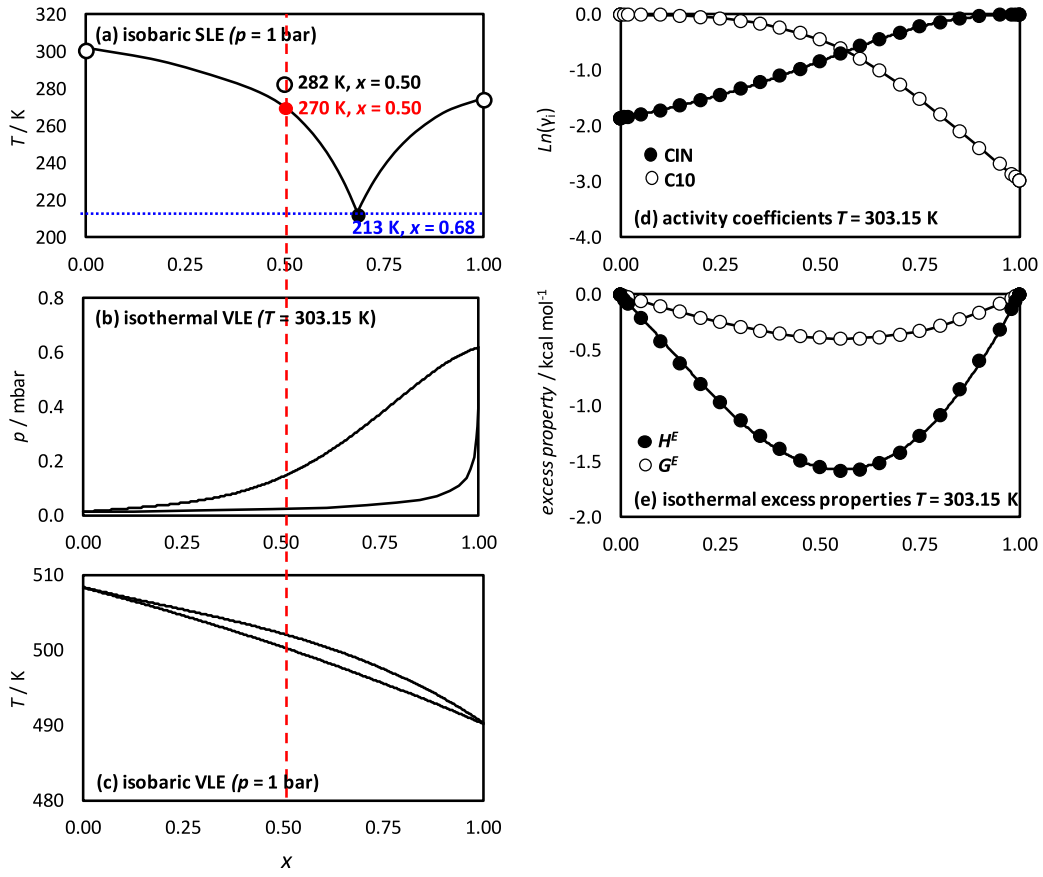

Fig. 2. Thermodynamic properties for × CIN: (1-*x*) C10 mixtures obtained from COSMO-RS calculation. Results include Solid-Liquid (SLE) and Vapor – Liquid (VLE) equilibria, as well as activity coefficients (γ_i), excess enthalpy (H^E) and excess Gibbs energy (G^E). In panel a, black filled circle indicates COSMO-RS eutectic composition, red filled circle indicates COSMO-RS melting temperature for equimolar composition and black empty circles indicate experimental melting temperatures of pure compounds and equimolar composition obtained in this work. In panels a to c, red dashed line indicates equimolar composition considered in this work for the experimental and theoretical study. (For interpretation of the references to colour in this figure legend, the reader is referred to the web version of this article.)

hydrogen bonding is inferred from the thermodynamic results in Fig. 2, these interactions are weakened at the vacuum interface because of the enrichment in CIN molecules, and thus the decrease in C10 / CIN ratio leads to decrease in hydrogen bonding extension and to low IFT. The pressure profile across the interface, Fig. 3b, indicates a moderate peak corresponding to the IFT value. In the case of DES – water interface, the behavior is inverse to the one at vacuum interface: a C10 – rich interface is inferred, which may be justified considering the competing effect of C10 – water hydrogen bonding with C10 – CIN ones. In spite of the hydrophobic character of bulk CIN: C10 (1: 1) DES, the water interface region is enriched in the organic acid because of its suitability for acting both as HBA and HBD with water molecules. This surface enrichment in decanoic acid has been previously reported from MD simulations at water interface of type iii and type v hydrophobic DES [69], and it leads to interface structuring very different to the bulk liquid phase one, and it needs to be considered to analyze relevant applications such as liquid–liquid equilibria or solutes extraction from water liquid phases. The pressure profiles across the water interface, Fig. 3d, are indicate a positive peak at the DES side and negative one at the water side, which agrees with the disruption of the DES self-structuring via the development of new interactions with water molecules, leading to low IFT as reported in the literature [69]. Considering the hydrophobic character and at the same time the heterogeneities appearing at the interface region, the ability of CIN: C10 (1: 1) for absorbing atmospheric water was experimentally measured, Fig. 4. In spite of the affinity for water molecules at the interface region, the saturation amount of absorbed water is remarkably low (0.341 wt%), which confirms that the affinity for water molecules is a local effect at the interface whereas the bulk liquid phase has not a large trend to host water molecules, thus leading to low water solubility. Nevertheless, the saturation conditions are reached in a short time exposure as indicated by the calculated kinetic constant. Therefore, the considered DES can be exposed to open atmosphere conditions without large changes in its properties, which is of great relevance considering the well-known disrupting effect of water on many types of DES [70,71], and it shows again the advantageous properties of hydrophobic DES. Likewise, the use of type *v* hydrophobic NADES, absent of halide ions, does not lead to the possible development of acidic water phases with high halide, which may a problem both from technical and environmental viewpoint [72].

Another relevant topic on the suitability of the proposed DES for its large-scale use is its environmental and toxicological behavior. The properties reported in Fig. 3c, 3d and 4, indicates both minor impact of water on DES properties but also low impact of the considered DES on water, thus minimizing its impact on natural water sources. To analyze its possible toxicological effects, considering a first approach, its interaction with lipid bilayers as models of cell (plasma) membranes because cell wall disruption may be considered as a possible MIE for the AOP of the studied DES. For this purpose, the use of COSMOperm approach allows a quantification of the properties of the considered DES at cell membranes modelled as a systems formed by a POPC lipid bilayer. Although this is a sim-

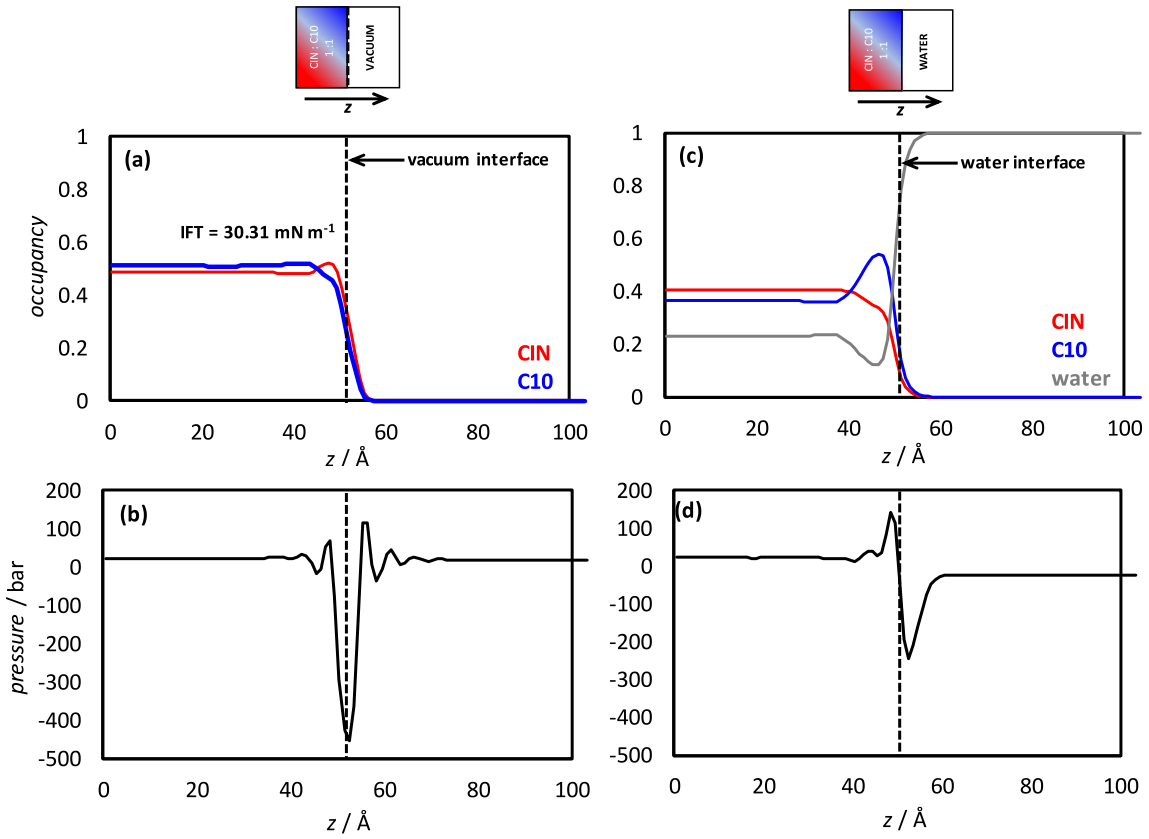

Fig. 3. Properties of (a,b) CIN: C10 1: 1 – vacuum interface and (c,d) CIN: C10 1: 1 – water interface as calculated from COSMOplex method. Panels a,c shows molecular distribution in the direction perpendicular to the interface (dashed line); panels b,d shows internal pressure profile across the interface. IFT stands for calculated interface tension. All values reported at 303 K.

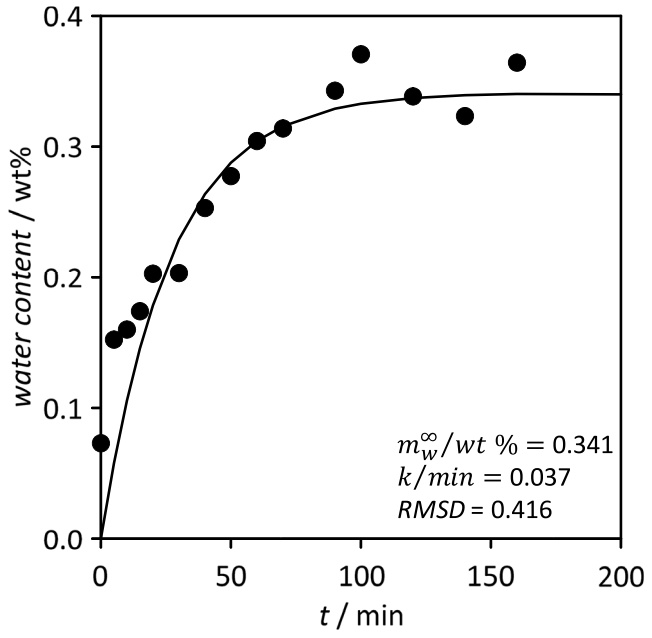

Fig. 4. Kinetics for atmospheric water absorption in CIN: C10 (1: 1) DES at 298 K. Lines show fitting to the kinetic model, eq. (1), with the parameters reported at the bottom of the Figure.

plified approach, it may lead to relevant insights on the behavior of the considered molecules in contact with cell environments, Fig. 5. The free energy profiles are reported in Fig. 5a for independent CIN and C10 molecules, and for the CIN: C10 pair, i.e. molecular structure corresponding to the DES in comparison with DES components. The reported results indicate larger changes in the free energy profiles upon formation of the molecular pair (CIN – C10) leading to DES formation. The model bilayer is formed by two well-defined different areas: the one on top corresponding to head polar groups of the lipid molecules and the central apolar region formed by the apolar hydrophobic chains. The reported results indicate a remarkable stabilization of the CIN – C10 pair in the central apolar region of the bilayer which results in a synergistic effect upon comparison with the behavior of independent CIN and C10 molecules. The free energy behavior results in the resistance to permeation reported in Fig. 5b, although a barrier to penetration close to the head polar groups is inferred both for the independent components and the CIN – C10 pair, this barrier is lower for the pair, i.e. penetration is favored, and a very low resistance is inferred once the CIN-C10 pair is placed in the central apolar region of the lipid bilayer. The calculated self-diffusion coefficients, Fig. 5c, for the molecules into the bilayer indicate low mobility once the CIN – C10 pairs are placed in the center of the molecule, in agreement with the low free energy reported in Fig. 5a, i.e. CIN-C10 pairs are able to develop efficient interactions with alkyl chains of lipid molecules, reducing molecular mobility, low self-diffusion coefficients, and thus, disrupting lipid-lipid self-interaction through alkyl chains. Therefore, CIN-C10 molecular pairs have a large permeability on the considered model lipid bilayer, Fig. 5d, and this large permeability is produced by a syner-

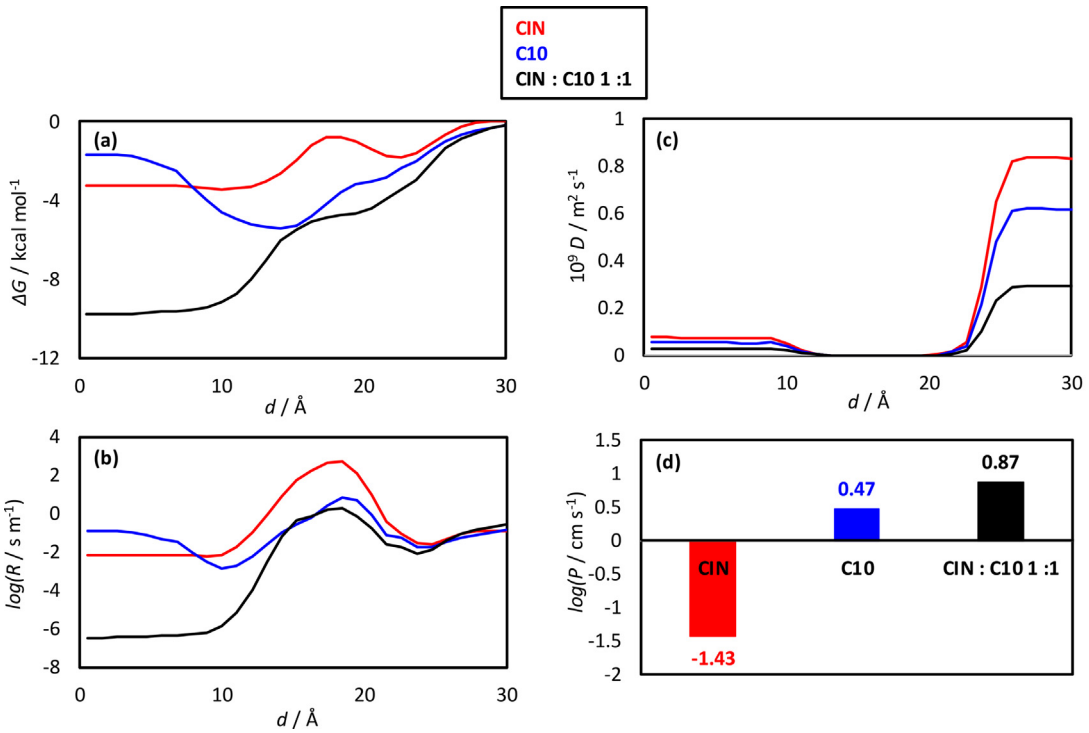

Fig. 5. Properties for the interaction of CIN, C10 and CIN: C10 1: 1 systems interacting with POPC lipid bilayer from COSMOperm calculations. Free energy profiles, ΔG, resistance, R, and self-diffusion, D, profiles are reported in panels a, b and c, respectively as a function of the relative position with regard to the bilayer center, d. Panel d show permeabilities, P. All values reported at 303 K.

gistic improvement in comparison with isolated CIN and C10 components, this increase in the effects on cells have been experimentally reported for several types of hydrophobic DES [20]. Therefore, the ability of CIN-C10 pairs to penetrate into the plasma membranes should lead to a disruptive effect on membranes properties.

Relevant thermophysical properties are also reported in this work for CIN: C10 (1: 1), Table S2 (Supplementary Information) and Fig. 6. The ρ and α_p values (Fig. 6a) shows a linear behavior in the considered temperature range (293.15 to 333.15 K). The density of the considered DES is remarkably lower than for water. Likewise, the available density data in the literature for hydrophobic DES are in the 0.89 to 1.1 g cm^{-3} range [73–75,81], and thus CIN: C10 (1: 1) stands in the low limit of the density range for the hydrophobic DES studied in the literature [74], which agrees with its large hydrophobic nature, i.e. the larger hydrophobicity the lower the density. This low density is even more remarkable when compared with density for type iii DES, e.g. archetypical choline chloride: urea (1: 2) hydrophilic DES shows 1.199 g cm^{-3} density at 298.15 K, which is 29 % larger than for CIN: C10 (1: 2). The hydrophobicity of the considered DES is quantified through the octanol–water partition coefficient as calculated using COSMOtherm being 3.10 (3.13 in [75]), 4.17 (4.09 in [76]) and 7.82 for logK_{ow} of CIN, C10 and CIN: C10 (1: 1), respectively. Therefore, hydrophobicity of the fluid is reinforced upon DES formation in comparison with independent components, and thus, very hydrophobic DES is prepared leading to low viscosity. The hydrophobicity of the DES is even larger than for pure *n*-decane alkane (logK_{ow} = 6.25 [76]), thus showing how combining two

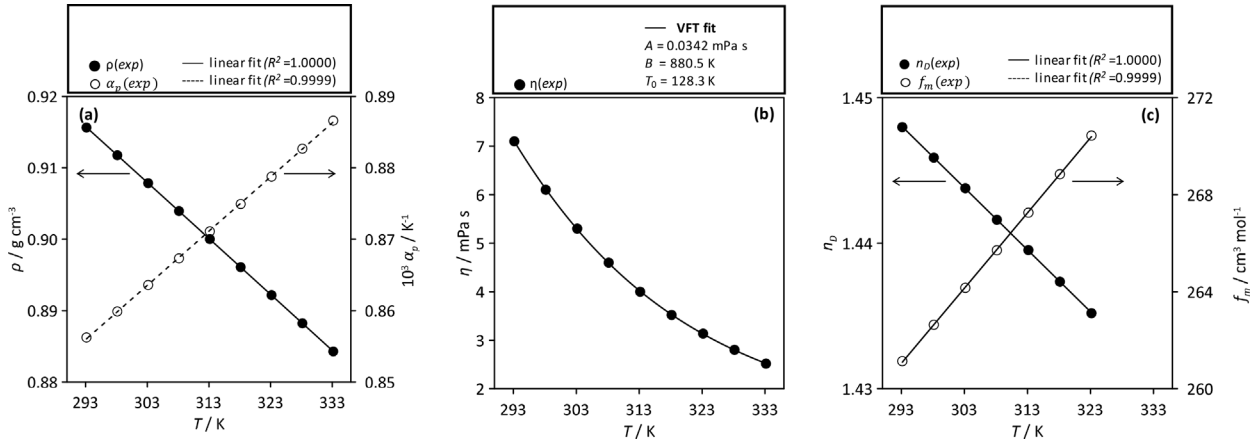

Fig. 6. Experimental thermophysical properties for CIN: C10 (1: 1) DES as a function of temperature, T. (a) Density, ρ, thermal expansion coefficient, α_p; (b) dynamic viscosity, η, refraction index; (c) n_D, and molar free volume, f_m. Linear fits and the corresponding coefficients of regression, R^2, are reported in panels a and b. Fit to Vogel-Fulcher-Tamman equation is reported in panel b.

moderately hydrophobic components leads to very hydrophobic DES, which produces a low dense fluid. Likewise, its low density leads to large thermal expansion coefficients, Fig. 6a, which results from the presence of large alkyl chains leading to chain to chain molecular packings, and thus forming holes into the liquid structure (i.e. the higher the thermal expansion coefficient, the higher the free volume). The thermal expansion coefficient for CIN: C10 (1: 1) at 298.15 K (0.810 10^{-3} K^{-1}) is in the same range of other type v hydrophobic DES (e.g. 0.80 for menthol: thymol (1: 1) [79]) and remarkably larger than for hydrophilic type iii DES (e.g. 0.437 10^{-3} $K^{-1}$for choline chloride: urea (2: 1) [77]). Moreover, the temperature evolution of thermal expansion coefficient for CIN: C10 (1: 1) follows a linear increasing trend upon heating but with just a 3.3 % change in the studied 293.15 to 333.15 K range, i.e. a slight increase in compressibility thus showing the fluid maintaining most of their volumetric features and molecular packing for the 40 K studied temperature range. The increase of thermal expansion coefficient upon heating is a common feature for DES both for type iii [77] and type v DES [80]. Although the positive slope of thermal expansion coefficients vs temperature is the common behavior of most fluids, it has been reported in the literature anomalous negative slopes for compounds closely related to DES such as imidazolium or pyridinium ionic liquids [78], in the case of DES, neither hydrophobic type iii DES, such as the one considered in this work, nor even imidazolium based hydrophilic DES [79] show negative slopes for thermal expansion coefficient vs temperature, and thus this anomaly seem to be absent in DES. As the thermal expansion coefficient may be related with the efficiency of molecular packing, i.e. with formation of holes (interstices), this effect is quantified through the approach developed by Yang et al. [80] for ionic liquids, which can be applied to closely related DES fluids. In this approach, the average volume of interstices, v, may be calculated from equation (7):

$$\alpha_p = \frac{3N_A v}{VT} \tag{6}$$

where V stands for the molar volume. The calculated v evolves in a linear trend from 49.5 $Å^3$ (cavities of 2.28 Å radius) at 293.15 K to 60.4 $Å^3$ at 333.15 K, i.e. slightly larger interstice volumes are inferred. Likewise, the volume percentage of interstices, i.e. the contribution of interstices (holes) to the total molar volume evolves from 25 % at 293.15 K to 30 % at 333.15 K, thus, large interstices volumes are inferred (e.g. 10 to 15 % are obtained for related fluids such as ionic liquids [80]), which slightly increase upon heating. Therefore, large available empty space is inferred from the measured volumetric properties.

An additional remarkable result is the very low viscosity of CIN: C10 (1: 1) DES, being one of the less viscous hydrophobic DES reported in the literature [74]. This low viscosity is a remarkable advantage for the application and scaling up of this fluid as it will lead to more efficient heat and mass transfer operations. The viscosity vs temperature behavior shows a non-Arrhenius evolution and thus it was fitted to VFT model. The VFT fitting parameters allowed the calculation of D_f fragility parameter (=6.9), which allow to classify the fluid as fragile (D_f < 30 [81]), which can be justified considering that the structural properties of the considered fluid are mainly determined by van der Waals interactions between the available long alkyl chains in C10, which can be disrupted considering its strength. The fragility of CIN: C10 (1: 1) hydrophobic DES is larger (lower D_f) than for hydrophobic type v DES not containing long chain acids (e.g. those formed only by monoterpenoids combination with D_f in the 9 to 42 range [35]) and also lower than for type iii DES (e.g. D_f = 18.9 for choline chloride: ethylene glycol 1: 2 [82]). Two main effects should control the viscosity of the studied hydrophobic NADES: i) intermolecular forces between CIN-C10 pairs, and ii) molecular mobility as controlled by the availability of empty spaces (as quantified from the obtained interstices volumes) and their dynamics. It is found a close to linear correlation (R^2 = 0.98) between experimental viscosity and the average volume (size) of interstices, thus confirming a pivotal role on the availability of interstices for improving molecular mobility, and thus decreasing fluids viscosity, i.e. the presence of long alkyl chains beyond conferring an hydrophobic nature to the fluid controls the molecular packing, leading to a large available empty space resulting in low viscosity. Regarding the measured refraction index, Fig. 6c, a linear behavior is also inferred upon heating, with the measured low refraction index corresponding to large free volume, in agreement with the large compressibility of the fluid as a results of the presence of long alkyl chains. Moreover, a linear relationship has been obtained (R^2 = 1.00) between experimental refraction index and thermal expansion coefficient showing how this optical property also quantifies the effectiveness of molecular packings in the considered fluid.

The Raman spectra for the isolated components as well as for the DES are reported in Fig. 7a. The full spectral assignment is out of the scope of this work as the objective of these measurements were to infer the possible changes in the spectra upon DES formation. Nevertheless, several relevant Raman spectral features appear for pure CIN and C10 before DES formation. In the case of CIN, Fig. 7a, a intense and narrow peak is obtained at 638 cm^{-1} which corresponds to the characteristic ring deformation (δ(ring), reported at 652 cm^{-1} in the literature [83,84]) as well as a peak at 1433 cm-1 corresponding to CH deformation modes (reported at 1446 cm-1 in the literature [85]). In the case of neat C10, several relevant peaks are inferred: i) 878 cm^{-1} (CH_2 rock), ii) 1061 cm^{-1} (C—C stretch), iii) 1292 cm^{-1} (CH_2 twist), iv) 1430 cm^{-1} (CH_2 wagging, scissoring and deformation) and v) 1656 cm^{-1} (CO stretch, with weak intensity because of the involvement in hydrogen bonding [86]); these peaks are in agreement with literature results [87].Raman spectroscopy studies (laser excitation wavelength of 532 nm in comparison with 785 nm used in this study) on the tetrabutylammonium chloride: decanoic acid 1: 1 type iii hydrophobic DES have been reported in the literature [88]. This study showed that the Raman spectra for tetrabutylammonium chloride: decanoic acid DES is not exactly the sum of the spectra of the corresponding neat components with larger contribution for the tetrabutylammonium chloride although this effect is only showed in the region between 2900 and 3000 cm^{-1}. The main peaks for CIN and C10 below 2800 cm^{-1} were analyzed to see if some of them is remarkably different to the sum of both components, results in Fig. 7b indicate that the measured Raman spectra (in the region up to 2800 cm^{-1}, i.e. stretching vibrations of C10-OH groups appearing around 3100 cm^{-1} are not considered) are mostly a combination of those of independent components, with a main effect resulting in the increase of the intensity of the most relevant peaks but with peak positions remaining unchanged. As the peaks appearing below 2800 cm^{-1} mostly correspond to vibrations involving CH_2 groups, and these groups are involved in dispersion intermolecular interactions, it may be concluded that dispersion interactions are similar in the DES as in the neat independent CIN and C10. Considering the large number of CH_2 groups in C10, the structure of the DES should be determined by alkyl – alkyl chain dispersive interactions, which would justify the reported thermophysical properties as well as the availability or interstices. The Raman peak position for CO stretching does not change on going from neat C10 to DES, as CO group is only involved in hydrogen bonding as acceptor (i.e. C10 – C10 self-hydrogen bonding via CO – OH interactions) it may be concluded that C10 self-interaction via CO groups is not changed upon DES formation. Likewise, as the formation of the DES involves the development of CIN – C10 heteroassociations via hydrogen bonding between the C10(OH) and CIN(O) groups, to characterize this new interaction

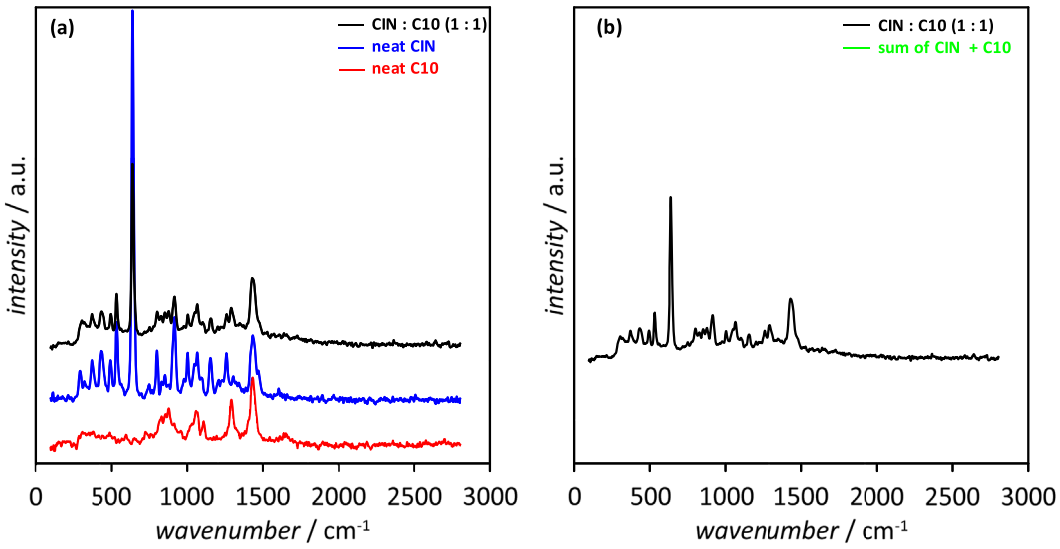

Fig. 7. Raman spectra of CIN: C10 (1: 1) DES, neat CIN and neat C10 at 298.15 K. Panel b shows Raman spectra for the CIN: C10 (1: 1) DES as well as the sum of spectra for neat CIN + neat C10 to compare with the spectrum for the formed DES.

upon DES formation vibrations involving CIN(O) ether group were considered, and for that purpose vibrations involving CIN(O—C) were analyzed, the vibrations of the two CIN(O—C) bonds appear at 916 and 800 cm^{-1} both in the neat CIN as well as in the DES. The main change in the properties of CIN(O—C) bands stands on the decrease of their intensity on going from neat CIN to DES, which may be attributed to the formation of hydrogen bonding with the C10 molecules. Therefore, the structure of the liquid beyond the formation of CIN – C10 hydrogen bonds competing with those C10-C10, is similar those in neat independent fluids and mainly determined by the strong trend of alkyl chains to self-associate forming large hydrophobic domains. Regarding the possible effect of the laser excitation wavelength on the obtained Raman spectra, it is well-known that the shorter the wavelength the larger the stronger the induced fluorescence background, whereas longer wavelengths lead to larger thermal effects, but without relevant effects on the position of the obtained peaks [89]. Therefore, the considered excitation wavelength (785 nm) may be considered as a compromise solution to optimize both effects in the considered DES.

The analysis of intermolecular forces was firstly considered using DFT theoretical approach for CIN – C10 dimmers (minimal model for hydrogen bonding in the considered fluid), Fig. 8. The analysis of HBA – HBD hydrogen bonding in hydrophobic DES via DFT approach is still scarce in the literature. Fan et al. [90] studied terpene-based hydrophobic DES reporting HBA – HBD interaction energies in the 19.9 to 41.6 kJ mol^{-1} range, with CVBs in the −0.01 to −0.04 range for the hydrogen bonding sites. Gutierrez et al. [91] carried out DFT studies on archetypical hydrophobic DES such as menthol: thymol and those formed by these monoterpenoids and levulinic acid reporting interaction energies in the 27.7 to 51.7 kJ mol^{-1} range with the QTAIM and NCI analysis indicating the formation of strong hydrogen bonds. Additional literature studies [35] on monoterpenoid – based hydrophobic DES confirmed using DFT the formation of strong hydrogen bonds, although those combining only monoterpenoids have lower interaction energies (roughly 20 kJ mol^{-1}) and larger (positive) CVB indices than those conspiring the combination of monoterpenoids and e.g. organic acids (binding energies larger than 50 kJ mol^{-1} [79]). It should be remarked that the HBA – HBD interaction energy as obtained from DFT calculation for hydrophobic type v DES is in the same range as for common type iii hydrophilic DES, e.g. this energy for the archetypical choline chloride: urea 1:2 corresponding to the HBA – HBD interaction is roughly 45 kJ mol^{-1} [92]. For CIN – C10 hydrogen bonding, the calculated ΔE is remarkably large indicating strong interaction. This hydrogen bonding is identified through QTAIM as the formation of a BCP between the donor and the acceptor and a bond path between both sites. The BCP corresponding to the hydrogen bond is characterized by the ρ and $\nabla^2\rho$, Fig. 8a. According to Popelier and Koch [93] hydrogen bonds are characterized by BCPs with ranges (0.002 to 0.035 a.u) and (0.024 to 0.139 a.u.) for ρ and $\nabla^2\rho$, respectively, with larger values corresponding to stronger interactions, and thus, the CIN – C10 hydrogen bond may be classified as a very strong interaction from the topological viewpoint in agreement with the large ΔE. Likewise, the optimized structure for CIN – C10 dimmer indicates that beyond the strong hydrogen bond, CIN and C10 molecules also interact through the C10(CO) and CIN(CH_3) groups, as inferred by the formation of another BCPs with low but non-negligible ρ and $\nabla^2\rho$. The NCI analysis also confirms this mechanism of interaction, the strong localized blue spot in the C10(OH) to CIN(O) path is accompanied by a large interaction region corresponding to van der Waals like interactions. Moreover, the largely negative CVB for the developed hydrogen bonding (Fig. 8a) as well as the highly localized and intense spot from IRI analysis (Fig. 8b) confirm the hydrogen bonding development, and thus, indicate this effect as the pivotal interaction on the CIN – C10 DES formation. Moreover, the very strong hydrogen bonding between CIN and C10 molecules would be the justification for the very low volatility of the CIN: C10 (1: 1) DES, Fig. 2b and 2c, as well as for the ability of these molecular pairs to penetrate lipid bilayers, Fig. 4d. Beyond the prevailing role of intermolecular hydrogen bonding in DES properties, the presence of large alkyl chains from C10 molecules would lead to alkyl – alkyl van der Waals interactions, which although being weaker than the developed hydrogen bonding they should be relevant considering their additive character and the presence of a large number of methyl and methylene groups. With the objective of quantifying these van der Waals like interaction, tetramer models were built and optimized, Fig. 9. Two different types of tetramers were build considering different possible mechanisms of

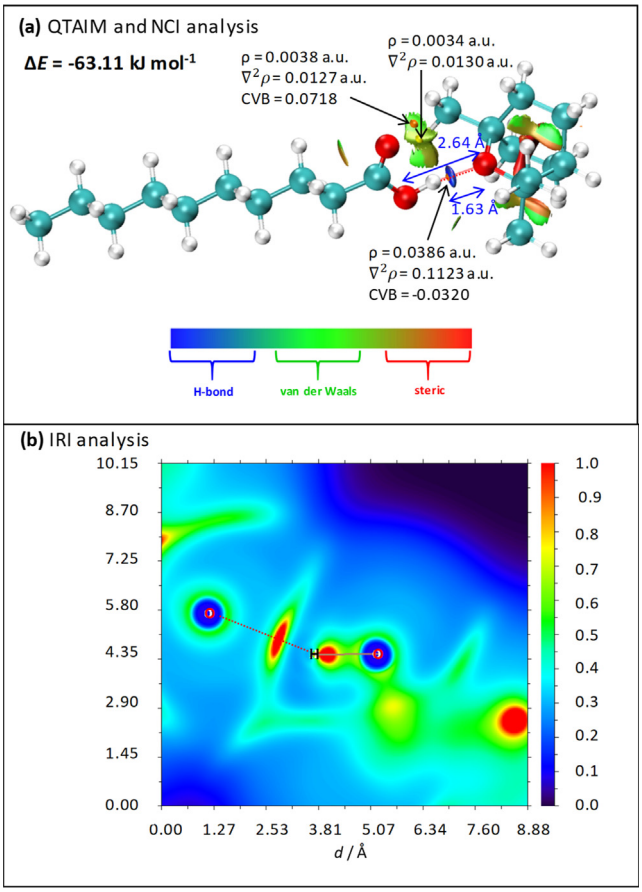

Fig. 8. DFT results for CIN – C10 dimmer showing (a) QTAIM and NCI analysis and (b) IRIS analysis of the intermolecular hydrogen bonding region. QTAIM analysis shows relevant BCPs (orange spheres) and RCPs (yellow sphere) in the region around the intermolecular hydrogen bond, indicating electron density (ρ) and the corresponding Laplacian ($\nabla^2\rho$). Core-Valence Bifurcation index (CVB) is also reported for the region corresponding to relevant intermolecular interactions. IRI analysis is reported for the region corresponding to the O(CIN) / O—H(C10) hydrogen bonding. Counterpoise corrected interaction energy, Δ*E*, is also reported. (For interpretation of the references to colour in this figure legend, the reader is referred to the web version of this article.)

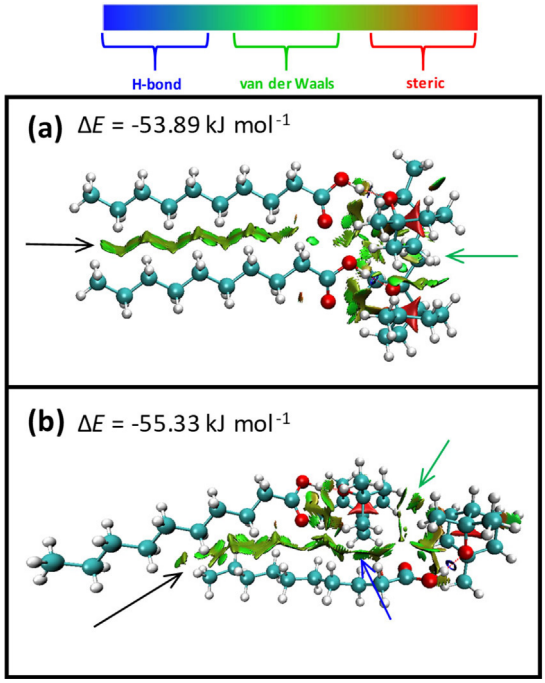

Fig. 9. DFT results for CIN – C10 tetramer showing NCI analysis. Arrows indicate areas corresponding to (black) alkyl chain – alkyl chain, (blue) CIN – alkyl chain and (green) CIN – CIN interactions, for the two lowest energy structures. Δ*E* stands for the counterpoise corrected interaction energy after removing contributions for the two CIN – C10 hydrogen bonds. (For interpretation of the references to colour in this figure legend, the reader is referred to the web version of this article.)

interactions between neighbor dimmers in the fluid: i) tetramer with C10 – C10 total interactions (i.e. overlapping of full alkyl chains, Fig. 9a) and ii) partial overlapping between C10 alkyl chains accompanied by CIN – C10 (alkyl) interactions, Fig. 9b. The binding energy (removing hydrogen bonding contribution) corresponding to van der Waals like interaction are remarkably large for both types of tetramers indicating how these intermolecular interactions would develop a pivotal role in the structuring in the liquid state, i.e. large trend to develop hydrophobic alkylic domains accompanied by CIN-C10 hydrogen bonding. The NCI analysis show intense regions of interactions corresponding to van der Waals interaction both of C10(alkyl) - C10(alkyl) and C10(alkyl) – CIN interactions corresponding to the strong molecule to molecule interactions.

The theoretical analysis of bulk liquid phases was carried out from MD simulations. The considered polarizable forcefield (AMOEBA09) was validated for this hydrophobic DES by the comparison of predicted and experimental density, Figure S2 (Supplementary Information). Predicted density data are in excellent agreement with experiments, with a slight overprediction but deviations lower than 0.6 %, but with slope of density vs temperature in fair agreement ($(\partial\rho/\partial T)_p = -7.8 \times 10^{-5} and -7.7 \times 10^{-5}$ g cm^{-3} K^{-1}, for experimental and MD predicted density, respectively), therefore, the forcefield can be considered as suitable for describing the fluid properties. Radial Distribution Functions (RDFs) for relevant atomic sites (those leading to hydrogen bonding) are reported in Fig. 10 for CIN – C10 heteroassociations (Fig. 10a) and C10 – C10 homoassociations (Fig. 10b). RDF for C10(OH) – CIN(O) interaction show two peaks, the first one, being very intense and narrow, with a maxima at 2.84 Å (slightly larger than the value obtained from DFT calculations of dimmers, Fig. 8) confirming hydrogen bonding in the bulk liquid phase. The second peak for C10(OH) – CIN(O) interaction indicates the interaction with neighbor interacting pairs as in DFT models (Fig. 9). Likewise, the peak for C10(CO) – CIN(O) interaction also confirms the development of additional interactions beyond the direct hydrogen bonding as in Fig. 8. The C10 molecules are also able to be self-hydrogen bonding and this is confirmed by results in Fig. 10b through the first narrow peak corresponding to C1O(OH) – C10 (CO) RDFs, whereas the hydrogen bonding between the C10(OH) – C10(OH) are produced in a minor extension as indicated by the weak first narrow RDF peak. Therefore, the bulk liquid phase is characterized both by C10 – CIN and C10 – C10 hydrogen bonding, with this last one being developed through hydroxyl and carbonyl groups, as well as by the presence of van der Waals like interactions. The molecular arrangements are also analyzed through Spatial Distribution Functions (SDFs) around CIN (Fig. 11a) or around C10 (Fig. 11b). For central CIN molecules, a spot indicating the highly localized arrangement of C10(OH) group around the CIN (O) atom is inferred with the C10(CO) groups placed around them. Likewise, C10(COOH) groups are placed around the apolar areas of the CIN molecule, confirming van der Waals interactions as inferred from DFT results (Fig. 9). The SDF around central C10 molecule show how hydrogen bonding with C10 molecule for neighbor C10 molecules is formed, as inferred from the well localized spots around the C10(COOH) groups. Moreover, CIN(O) atoms competing with O atoms in C10 as acceptors are accompanied a

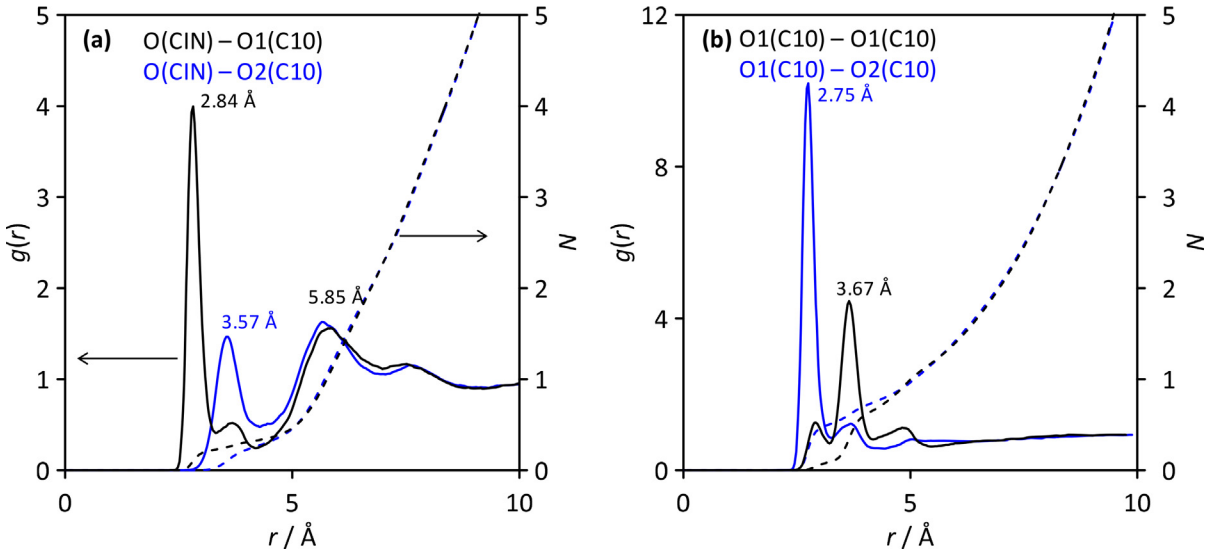

Fig. 10. Site-site radial distribution functions, $g(r)$, for the reported atomic pairs (labelling as in Fig. 1a) for CIN: C10 (1: 1) DES from MD simulations at 333 K and 1 bar. The values of the integrated $g(r)$ functions, N, are also reported. Label inside each panel indicate the position of relevant peaks.

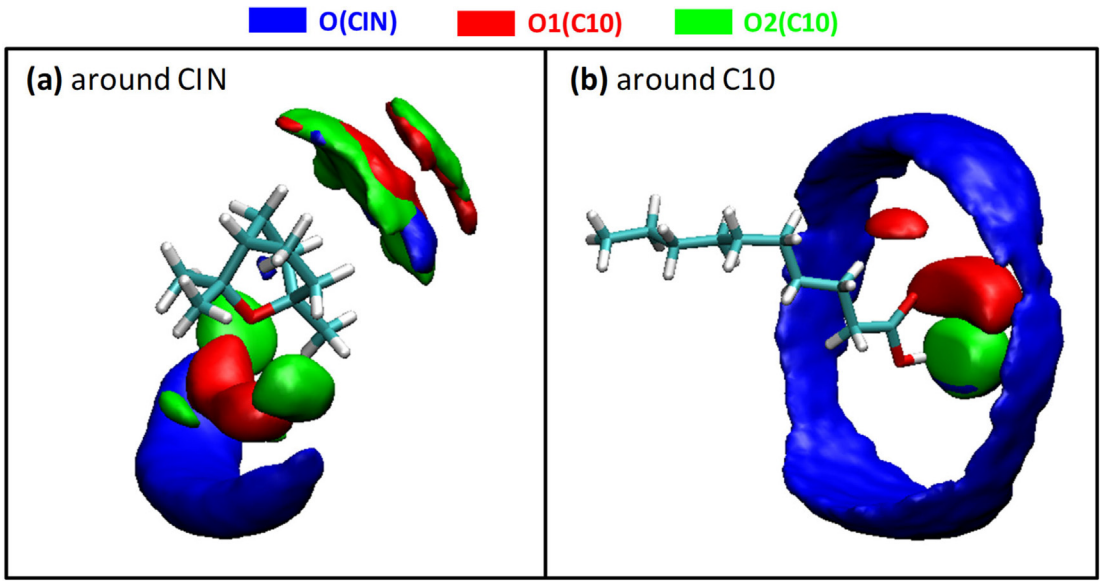

Fig. 11. Spatial Distribution Functions around (a) CIN and (b) C10 molecules for selected atoms in CIN: C10 (1: 1) DES from MD simulations at 333 K and 1 bar. Atom labelling as in Fig. 1a.

distribution of CIN molecules around the C10(COOH) group, i.e. CIN molecules in hydrogen bonding and non-hydrogen bonding situations are developed around C10, which corresponds to the two first RDF peaks reported in Fig. 10a. The extension of non-hydrogen bonded CIN molecules around C10 is non-negligible, as inferred from the extension of SDF (blue crown around the COOH) and from the integration of RDFs reported in Fig. 10a.

The properties of the developed different hydrogen bonds are analyzed through the Combined Distribution Functions (CDFs), which consider both the hydrogen bond distance as well as the corresponding donor – acceptor angles, Fig. 12. Reported CDFs show the maxima for CIN(O1) – C10(OH) corresponding at hydrogen bonding distance and a second spot at larger distances (corresponding to the two first peaks in RDF, Fig. 10a), both with a large linear interaction (maxima at 175°) Fig. 12a. Regarding the C10 (OH) – C10(OH) interaction, Fig. 12b, three spots are inferred form increasing distance corresponding to the three RDFs peaks reported in Fig. 10b, with the one corresponding to the shortest contact (hydrogen bonding) being linear and the second one showing high deviations from linearity. In the case of C10(OH) – C10 (CO) interaction two peaks are also inferred corresponding both ones to linear interactions. Therefore, all the possible interacting pairs form hydrogen bonding as inferred from CDFs, although their extension is not equivalent as inferred from the corresponding RDFs. The hydrogen bonding extension was quantified considering a geometric criteria both for homo and heteroassociations, Fig. 13. The reported results indicate that the number of C10-C10 hydrogen bonds is 50 % larger than C10-CIN ones, therefore upon the formation of the DES a large population of self-hydrogen bonded C10 molecules remain in the fluid in parallel with those C10 molecules interacting with CIN, with both types of interaction competing for the same donor sites in the acid, Fig. 10b. The temperature effect on both types of interactions is not very large, upon heating to 333 K the extension of hydrogen bonding decreases (more for

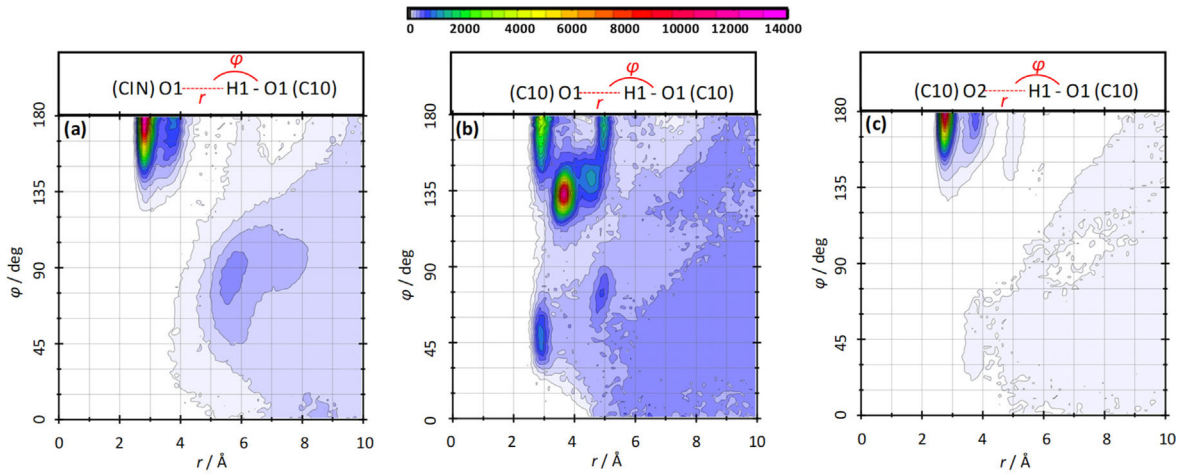

Fig. 12. Combined Distribution Functions for the distance and angles between relevant sites in CIN: C10 (1: 1) DES from MD simulations at 333 K and 1 bar. Atom labelling as in Fig. 1a.

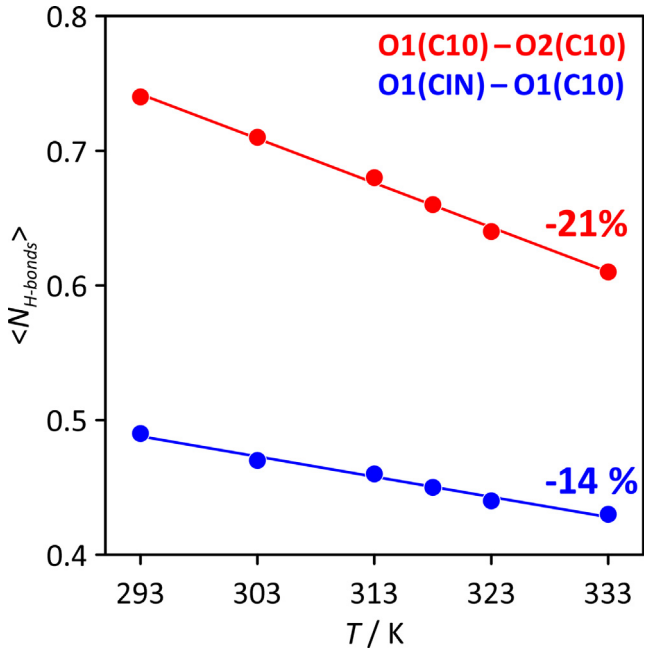

Fig. 13. Average number of hydrogen bonds per C10 molecule, $<N_{H\text{-}bonds}>$, for the reported atomic pairs in CIN: C10 (1: 1) DES from MD simulations as a function of temperature and 1 bar. Atom labelling as in Fig. 1a. Hydrogen bonding criteria: 3.5 Å and 60° as donor – acceptor distance and angle. Values inside the Figure indicate the decrease in $< N_{H\text{-}bonds} >$ on going from 293 to 333 K. Atom labelling as in Fig. 1a.

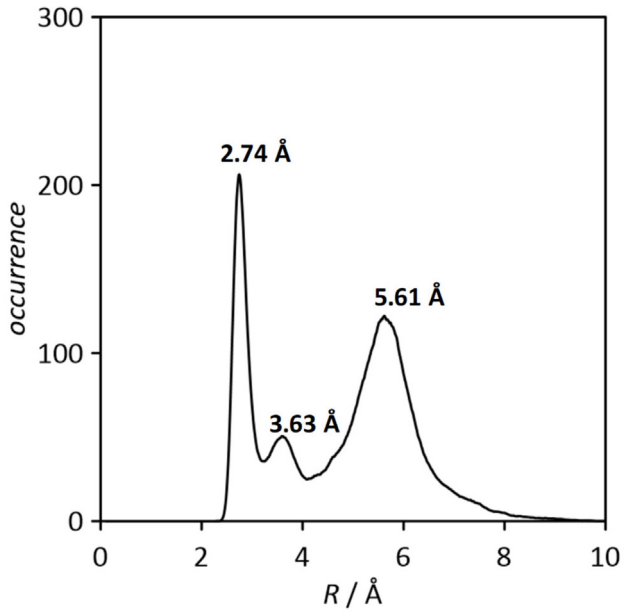

Fig. 14. Cluster analysis for hydrogen bonding sites in CIN: C10 (1: 1) DES from MD simulations at 303 K and 1 bar. Results show occurrence of possible clusters formed by O1(C10) as hydrogen bond donor and O(CIN), O1(C10) and O2(C10) as acceptors as a function of distance, *R*.

C10-C10 ones) but a large number of hydrogen bonds is inferred, which justified the minor trend to evaporate of the considered fluid, Fig. 2b and 2c.

Considering that C10 molecules develop hydrogen bonds both with CIN and C10 molecules a cluster analysis for these hydrogen bonding interactions was performed, Fig. 14. The reported cluster distribution show two intense peaks and a weaker one, with the most intense corresponding to 5.61 Å. Therefore, the size of hydrogen bonded clusters is not very large, and thus, a fluid structure formed by small hydrogen bonded sites dispersed in apolar hydrophobic domains would be present in the fluid. This is confirmed by the molecular distribution reported in Figure S3 (Supplementary Information), which indicate the presence of large apolar domains interconnected between CIN domains.

The reported experimental and predicted density data as well as the fluid's compressibility showed a low dense, largely compressible fluid, with interstices formation, therefore the extension of cavities distribution is also analyzed from MD simulations. Results in Fig. 15a show the cavity size distribution, showing a maxima for 0.58 Å cavity radius with an isoperimetric ratio of 0.86 (close to unit) indicating highly symmetrical, close to spherical cavities. Beyond the maxima of the cavity size distribution function, results in Fig. 15a indicate the availability of cavities with radius up to roughly 2.2 Å, i.e. cavities with volumes up to roughly 45 $Å^3$ which agrees with the interstices obtained from experimental properties. These cavities are larger than for related fluids such as dense ionic liquids (densities larger than 1) [94], which probes again the availability of empty space in the considered DES. Therefore, a relevant populations of cavities is present in this hydrophobic DES in agreement with experimental results, which is important for applica-

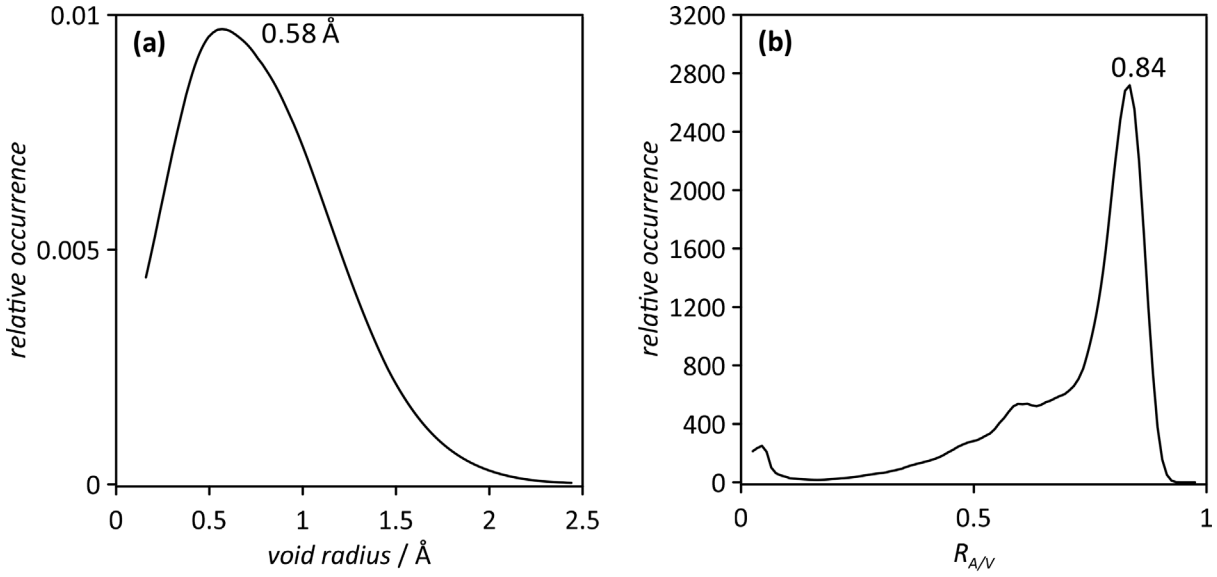

Fig. 15. Analysis of void distribution in CIN: C10 (1: 1) DES from MD simulations at 333 K and 1 bar. Panel a shows distribution of cavities as a function of cavity radius, panel b shows distribution of isoperimetric ratio for cavities, $R_{A/V}$.

tions such as gas solubility or solutes extraction applications. An additional analysis of the distribution inside the considered DES is carried out through the domain analysis for CIN and C10 molecules as well as for the domains corresponding to CIN – C10 hydrogen bonds, Table 1. The reported results indicate large domains of isolated CIN and C10 molecules, in agreement with results in Figure S3 (Supplementary Information). The domain count for CIN – C10 hydrogen bonds indicates that these domains are isolated, i.e. as results indicate large CIN and C10 domains these are only connected through (isolated) points where CIN and C10 molecules develop hydrogen bonds, with the remaining parts of the fluid formed by large apolar domains of C10 alkyl chains and CIN to CIN interacting molecules. The concepts of holes distribution and free volume is of great relevance for the characterization of fluids properties and relevant work has been previously carried out for ionic liquids, which can be compared with the behavior of DES as the one considered in this work. Beichel et al. [95] carried experimental studies for the determination of free volume and showed its relevance for the prediction of relevant physicochemical properties such as dynamic viscosity or electrical conductivity. These authors concluded that the hole free volume, as inferred in this work from experimental and MD studies, determines dynamic properties and thus it is a pivotal property for fluids characterization. Brooks et al. [96] also carried out studies on free volumes for ionic liquids and confirming the pivotal role of holes size on deviations from ideality. Therefore, the concept of holes distribution and sizes is also proved in this work for DES and it may be used in future works for designing DES with larger holes, i.e. less viscous, less dense and more suitable for solubility and extraction purposes.

The dynamic properties of CIN: C10 (1: 1) DES were also considered. First, the dynamic of the developed hydrogen bonds was analyzed through the van Howe correlation functions, Fig. 16. The dynamic behavior for CIN – C10 hydrogen bonding (Fig. 16a) indicates short living interactions, with interactions breaking for times shorter than 10 ps with an analogous behavior inferred for C10 – C10 interactions, Fig. 16b. Therefore, although the reported MD results indicate the formation of homo and heteroassociations via hydrogen bonding, these are short living interactions leading to a dynamical picture of the liquid structure with very fast breaking and reformation of the hydrogen bonding network, which would be on the roots of the macroscopic properties such as the very low viscosity, Fig. 6b. Center-of-mass Velocity Distribution Functions (VDFs) are reported in Fig. 17a showing curves with a single maxima appearing at higher values for CIN than for C10, i.e. velocities are faster for CIN than for C10 on average, which can be related with the ability of C10 molecules to develop hydrogen bonding with CIN and C10 molecules as well as due to the development of van der Waals like interactions between alkyl chains of C10 leading to apolar domains decreasing molecular velocity. Nevertheless, CIN velocities are only slightly larger than for C10 because of the interaction via hydrogen bonding with C10 as well as considering that CIN molecules are trapped among apolar C10 domains (Figure S3, Supplementary Information).

The calculated self-diffusion coefficients, *D* (Fig. 17b), obtained from the Mean Square Displacements (*msd*) are also reported showing faster diffusion for CIN molecules. Moreover, the reported *D* values are remarkably larger than for most of the literature studied DESs (roughly-two orders of magnitude faster diffusion rates), in agreement with the low viscosity for CIN: C10 (1: 1) DES [97,98], i.e. in spite of the formation of large hydrophobic domains because

Table 1
Domain analysis for CIN: C10 (1: 1) DES from MD simulations at 333 K and 1 bar. The domain count is reported with domain volume (D-Vol) and surface (D-Surf) as well as the isoperimetric quotient (Q^{per}).

unit	domain_count	D-Vol / Å^3	D-Surf / Å^2	Q^{peri}
CIN	1.0	44,684	24,083	0.13
C10	1.0	52,652	24,083	0.15
O1(CIN)-O1,H17(C10)	141	26	56	0.67

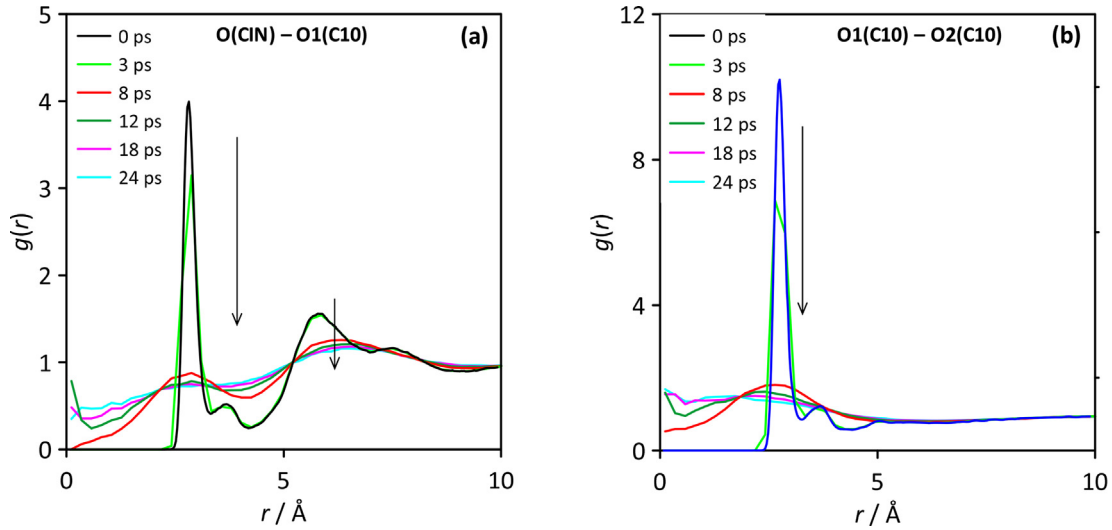

Fig. 16. Van Howe correlation functions for the reported atomic sites in CIN: C10 (1: 1) DES from MD simulations at 333 K and 1 bar. Arrows indicate increasing time for relevant peaks. Atom labelling as in Fig. 1a.

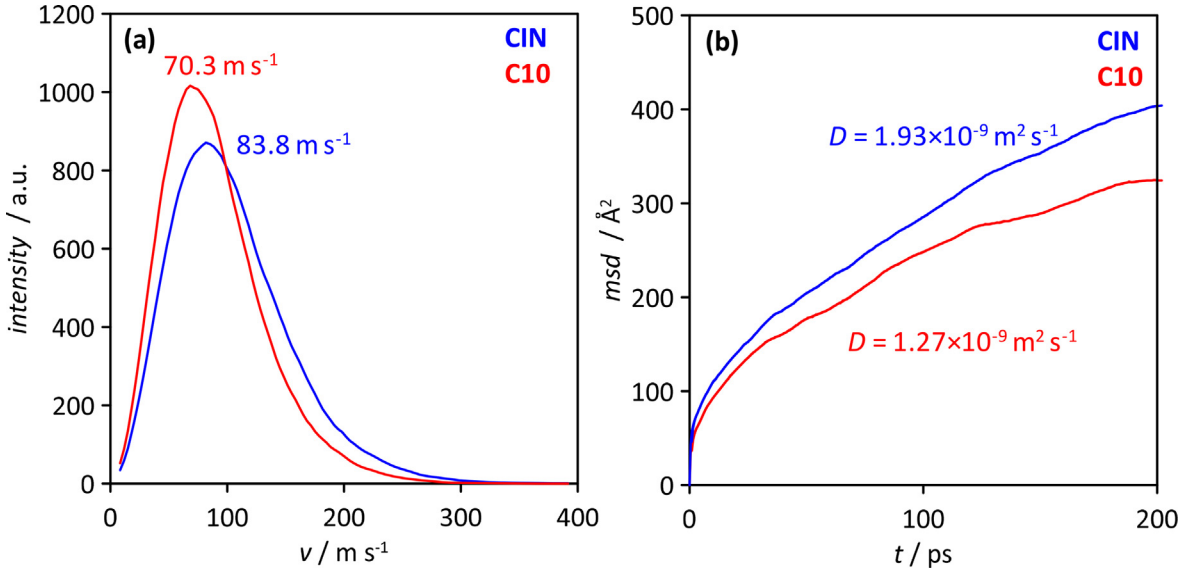

Fig. 17. (a) Velocity Distribution Functions and (b) Mean Square Displacements, *msd*, for CIN and C10 molecules in CIN: C10 (1: 1) DES from MD simulations at 333 K and 1 bar. Properties calculated for molecules center-of-mass. In panel b, self-diffusion coefficients calculated from *msd* are reported.

of the presence of long alkyl chains, a highly dynamic picture of the liquid structuring is inferred, which can also be justified considering the availability of free volume, favoring molecular mobility, as inferred from results in previous sections. The predicted self-diffusion coefficients were combined with the dynamic viscosity in the Stokes – Einstein equation to calculate the effective hydrodynamic radius of both type of molecules in DES leading to 0.50 and 0.77 Å for CIN and C10 molecules. These very low values are even smaller than the sizes of the isolated monomers, and analogous result have been reported for ionic liquids [99] as well as for hydrophobic DES [30], in which small hydrodynamic radius were justified considering the presence of heterogeneities in the studied fluids resulting in poor performance of the Stokes – Einstein which is known for fragile fluids as the DES considered in this work [30]. It should be remarked that the hydrodynamic radius for C10 in CIN: C10 DES at 333 K (0.77 Å) is even smaller than the value obtained for C10 in the tetrabutylammonium chloride: C10 hydrophobic DES (2.0 Å at 333 K), which corresponds to a larger viscosity and thus lower diffusion rates. The formation of nanoscopic heterogeneities reported in Figure S3 (Supplementary Information) is confirmed from MD results of dynamic properties.

Considering the prevailing role of C10 molecules in the structuring of the considered DES, vector autocorrelation functions for selected vectors in C10 were calculated, Fig. 18. First, the vector for the C10(OH) group is considered, which may be considered as a measurement of the stiffness for the hydrogen bonding network (both considering C10 – CIN and C10 – C10 interactions). A mono-exponentially decay is inferred, with fast reorientation in agreement with the van Howe results in Fig. 16. This fast reorientation dynamics indicate a low stiffness of the hydrogen bonding network as indicated in previous results. Likewise, the reorientation dynamics for the vector defined along the C10 alkyl chain (C1-10, Fig. 1) is slower than for the C10(OH) vector, therefore it is highly correlated with the C10(OH) reorientation and it is also fast, indicating also that the apolar domain reported in Figure S3 (Supplementary Information) are not rigid and suffer also remarkable reorientation.

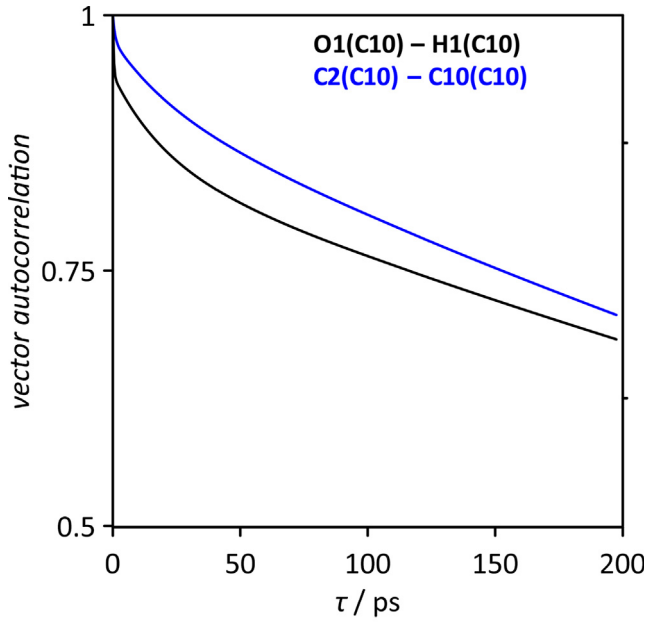

Fig. 18. Vector reorientation dynamics for relevant vectors of C10 in CIN: C10 (1: 1) DES from MD simulations at 333 K and 1 bar. Atom labelling as in Fig. 1.

Therefore, the extended and strong hydrogen bonding network formed by homo and heteroassociations as well as the presence of apolar domains via van der Waals interactions is accompanied by a fast evolution, reforming and reorientation of these interactions, leading to a highly dynamic picture for the fluid structuring.

4. Conclusions

The reported results provided an experimental and theoretical characterization of the properties, structuring and dynamics of the hydrophobic natural eutectic solvent formed by the combination of Cineole (as hydrogen bond acceptor) and decanoic acid (as hydrogen bond donor). The fluid properties are determined by the development of heteroassociations between cineole and decanoic acid as well as between decanoic acid molecules, these last ones remaining in remarkable extension upon the formation of the eutectic mixture. Likewise, the development of van der Waals like interaction between alkyl chains are also pivotal for determining fluid's structuring. These intermolecular forces lead to apolar and polar domains clearly separated in the fluid only connected through the sites where cineole and decanoic acid develop hydrogen bonds. Moreover, in spite of the formation of strong hydrogen bonds, the isolation of these interacting sites, especially for cineole – decanoic acid interactions, leads to highly dynamic interactions being reformed in the scale of a few picoseconds considering the rotational dynamics of the hydroxyl group in the considered acid. Likewise, apolar alkyl domains lead to cavities in the fluid and also suffer of fast reforming. These nanoscopic properties lead to a very low viscous and low dense fluid, with suitable properties for several technologies involving solubilization phenomena. The main factor that should be considered for the scaling up of this fluid is its suitability to penetrate and stabilize into cell membranes, which may lead to adverse outcome when living organisms are exposed to this hydrophobic deep eutectic solvent.

CRediT authorship contribution statement

Jose L. Trenzado: Conceptualization, Methodology, Resources, Writing – original draft, Writing – review & editing, Supervision. **Cristina Benito:** Investigation, Formal analysis, Data curation, Visualization. **Mert Atilhan:** Conceptualization, Methodology, Resources, Writing – original draft, Writing – review & editing, Supervision, Project administration, Funding acquisition. **Santiago Aparicio:** Conceptualization, Methodology, Resources, Writing – original draft, Writing – review & editing, Supervision, Project administration, Funding acquisition.

Data availability

Data will be made available on request.

Declaration of Competing Interest

The authors declare that they have no known competing financial interests or personal relationships that could have appeared to influence the work reported in this paper.

Acknowledgement

We acknowledge SCAYLE (Supercomputación Castilla y León, Spain) for providing supercomputing facilities. The statements made herein are solely the responsibility of the authors.

Appendix A. Supplementary material

Supplementary data to this article can be found online at https://doi.org/10.1016/j.molliq.2023.121322.

References

[1] T.A. El-Achkar, H. Greige-Gerges, S. Fourmentin, Basics and properties of deep eutectic solvents: a review, Environ. Chem. Lett. 19 (2021) 3397–3408.
[2] B.B. Hansen, S. Spittle, B. Chen, D. Poe, Y. Zhang, J.M. Klein, A. Horton, L. Adhikari, T. Zelovich, B.W. Doherty, B. Gurkan, E.J. Maginn, A. Ragauskas, M. Dadmun, T.A. Zawodzinski, G.A. Baker, M.E. Tuckerman, R.F. Savinell, J.R. Sangoro, Deep Eutectic Solvents: a review of fundamentals and applications, Chem. Rev. 121 (2021) 1232–1285.
[3] X.J. Hou, L.Y. Yu, C.H. He, K.J. Wu, Group and group-interaction contribution method for estimating the melting temperatures of deep eutectic solvents, AIChE J. 68 (2022) e17408.
[4] J. Liu, X. Li, K.H. Row, Development of deep eutectic solvents for sustainable chemistry, J. Mol. Liq. 362 (2022).
[5] C.M. Chabib, J.K. Ali, M.A. Jaoude, W. Alhseinat, I.A. Adeyemi, I.M. AlNashef, J. Water Process Eng. 47 (2022).
[6] Y. Liu, Z. Dai, Z. Zhang, S. Zeng, F. Li, X. Zhang, Y. Nie, L. Zhang, S. Zhang, X. Ji, Ionic liquids / deep eutectic solvents for CO_2 capture: reviewing and evaluating, Green Ener. Environ. 3 (2021) 314–328.
[7] N. Rodríguez, L. Machiels, B. Onghena, J. Spooren, K. Binnemans, Selective recovery of zinc from goethite residue in the zinc industry using deep-eutectic solvents, RSC Adv. 10 (2020) 7328–7335.
[8] M. Shaibuna, L.V. Theresa, K. Sreekumar, Neoteric deep eutectic solvents: history, recent developments, and catalytic applications, Soft Matter 18 (2022) 2695–2721.
[9] A. Misan, J. Nadpal, A. Stupar, M. Pojic, A. Mandic, R. Verpoorte, Y.H. Choi, The perspectives of natural deep eutectic solvents in agri-food sector, Critical Rev. Food Sci. Nut. 60 (2020) 2564–2592.
[10] S. Emani, A. Shanyanfar, Deep eutectic solvents for pharmaceutical formulation and drug delivery applications, Pharm. Develop. Technol. 25 (2020) 779–796.
[11] Y. Nahar, S.C. Thickett, Greener, Faster, Stronger: The benefits of deep eutectic solvents in polymer and materials science, Polymer 13 (2021) 447.
[12] M. Shi, W. Xiong, Z. Tu, X. Zhang, X. Hu, Y. Wu, Task-specific deep eutectic solvents for the highly efficient and selective separation of H2S, Separ. Sci. Technol. 276 (2021).
[13] S. Kaur, A. Malik, H.K. Kashyap, Anatomy of microscopic structure of ethaline deep eutectic solvent decoded through molecular dynamics simulations, J. Phys. Chem. B 123 (2019) 8291–8299.
[14] R. Gautam, N. Kumar, J.G. Lyman, Theoretical and experimental study of choline chloride-carboxylic acid deep eutectic solvents and their hydrogen bonds, J. Mol. Struc. 1222 (2020).
[15] G. García, M. Atilhan, S. Aparicio, An approach for the rationalization of melting temperature for deep eutectic solvents from DFT, Chem. Phys. Lett. 634 (2015) 151–155.

[16] L.J.B.M. Kollau, M. Vis, A. van den Bruinhorst, A.C.C. Esteves, R. Tuinier, Quantification of the liquid window of deep eutectic solvents, Chem. Commun. 54 (2018) 13351–13354.
[17] D.O. Abranches, J.A.P. Coutinho, Type V deep eutectic solvents: Design and applications, Curr. Opin. Green Sus. Chem. 35 (2022).
[18] Y. Liu, J.B. Friesen, J.B. McAlpine, D.C. Lankin, S.N. Chen, G.F. Pauli, Natural deep eutectic solvents: properties, applications, and perspectives, J. Nat. Prod. 81 (2018) 679–690.
[19] C. Florindo, L.C. Branco, I.M. Marrucho, Quest for green-solvent design: from hydrophilic to hydrophobic (deep) eutectic solvents, ChemSusChem 12 (2019) 1549–1559.
[20] J. Cao, E. Su, Hydrophobic deep eutectic solvents: the new generation of green solvents for diversified and colorful applications in green chemistry, J. Clean. Prod. 314 (2021).
[21] H.R. Salehi, A.T. Celebi, T.J.H. Vlugt, O.A. Moultos, Thermodynamic, transport, and structural properties of hydrophobic deep eutectic solvents composed of tetraalkylammonium chloride and decanoic acid, J. Chem. Phys. 154 (2021).
[22] D.P. Arcon, F.C. Franco, All-fatty acid hydrophobic deep eutectic solvents towards a simple and efficient microextraction method of toxic industrial dyes, J. Mol. Liq. 318 (2020).
[23] L. Sportiello, F. Favati, N. Condelli, M. Di Cairano, M.C. Caruso, B. Simonato, R. tilve, F. Galgano, Hydrophobic deep eutectic solvents in the food sector: Focus on their use for the extraction of bioactive compounds, Food Chem. 405 (2023) 134703.
[24] I. Wazeer, H.F.Hizaddin, M.A. Hashim, M.K MHadj-Kali, An overview about the extraction of heavy metals and other critical pollutants from contaminated water via hydrophobic deep eutectic solvents, J. Environ. Chem. Eng. 10 (2022) 108574.
[25] C.C. Chen, Y.H. Huang, J.Y. Fang, Hydrophobic deep eutectic solvents as green absorbents for hydrophilic VOC elimination, J. Hazar. Mat. 424 (2022).
[26] K. Xin, F. Gallucci, M. van Sint-Annaland, Development of natural hydrophobic deep eutectic solvents for precombustion CO_2 capture, ACS Sustainable Chem. Eng. 10 (2022) 15284–15296.
[27] A. Malik, H.S. Dhattarwal, H.K. Kashyap, An overview of structure and dynamics associated with hydrophobic deep eutectic solvents and their applications in extraction processes, ChemPhysChem 23 (2022) e202200239.
[28] K. Kongpol, P. Chaiao, P. Shuapan, P. Kongduk, W. Chunglok, G. Yusakul, Therapeutic hydrophobic deep eutectic solvents of menthol and fatty acid for enhancing anti-inflammation effects of curcuminoids and curcumin on RAW264.7 murine macrophage cells, RSC Adv. 12 (2022) 17443–17453.
[29] D.S. Juneja, S. Pandey, Water miscibility, surface tension, density, and dynamic viscosity of hydrophobic deep eutectic solvents composed of capric acid, menthol, and thymol, J. Chem. Eng. Data 67 (2022) 3400–3413.
[30] H. Kivela, M. Salomaki, P. Vinikka, E. Makila, F. Poletti, S. Ruggeri, F. Terzi, J. Lukkari, Effect of water on a hydrophobic deep eutectic solvent, J. Phys. Chem. B 126 (2022) 513–527.
[31] K. Zhu, q. Wei, K. Liu, M. Li, X. Ren, Design and combination of magnetic ionic liquids and hydrophobic deep eutectic solvents for safer extraction of titanium: physicochemical properties and toxicity studies, Green Chem. 24 (2022) 7481-7491.
[32] F. Oliveira, f. Santos, A.R.C. Duarte, Therapeutic deep eutectic systems towards the treatment of tuberculosis and colorectal cancer: opportunities and challenges, Molecules, 26 (2021) 7022.
[33] C. Florindo, F. Lima, L.C. Branco, I.M. Marrucho, Hydrophobic Deep Eutectic Solvents: A circular approach to purify water contaminated with ciprofloxacin, ACS Sustainable Chem. Eng. 7 (2019) 14739–14746.
[34] D.J.G.P. van Osch, C.H.J.T. Dietz, J. van Spronsen, M.C. Kroon, F. Gallucci, S. Annaland, R. Tuinier, A Search for Natural Hydrophobic Deep Eutectic Solvents Based on Natural Components, ACS Sustainable Chem. Eng. 7 (2019) 2933–2942.
[35] S. Rozas, L. Zamora, C. Benito, M. Atilhan, S. Aparicio, A study on monoterpenoid-based natural deep eutectic solvents, Green Chem. Eng. (2022), https://doi.org/10.1016/j.gce.2022.05.005.
[36] K. Yuan, F. Li, L. Peng, X. Zhao, H. Song, Separation of 1,8-Cineole and terpenes by Liquid-liquid extraction with green alkanediols, J. Mol. Liq. 350 (2022).
[37] Z. Shi, m. Wen, J. Zhao, M. Li, X. Han, Recent Advances in Biosynthesis of 1,8-Cineole, China Biotechnol. 38 (2018) 92-102.
[38] D. Mendham, D. Drew, A. Abadi, J. Bartle, A. Peck, D. Crawford, Potential cineole cost and availability from mallee eucalypt shelterbelt plantations in western Australia, CSIRO (2015), Australia.
[39] Y. Chen, Y. She, J. Lei, D. Wang, S. Wu, K. Men, Medium chain fatty acids: extraction, isolation, purification, bioactive properties and application, IOP Conf. Series: Earth and Environmental, Science 705 (2021).
[40] Z. Song, X. Hu, H. Wu, M. Mei, S. Linke, T. Zhou, Z. Qi, K. Sudmacher, Systematic Screening of Deep Eutectic Solvents as Sustainable Separation Media Exemplified by the CO_2 Capture Process, ACS Sustainable Chem. Eng. 8 (2020) 8741–8751.
[41] D. Peng, A. Alhadid, M. Minceva, Assessment of COSMO-SAC Predictions for solid–liquid equilibrium in binary eutectic systems, Ind. Eng. Chem. Res. 61 (2022) 13256–13264.
[42] J.A.H. Schwöbel, A. Ebert, K. Bitterman, U. Huniar, K.U. Goss, A. Klamt, COSMOperm: Mechanistic prediction of passive membrane permeability for neutral compounds and ions and its pH dependence, J. Phys. Chem. B 124 (2020) 3343–3354.
[43] T.E. Allen, J.M. Goodman, S. Gutsell, P.J. Russell, Defining molecular initiating events in the adverse outcome pathway framework for risk assessment, Chem. Res. Toxicol. 27 (2014) 2100–2112.
[44] T.M. Abdelghany, A.C. Leitch, I. Nevjestic, I. Ibrahim, S. Miwa, C. Wilson, S. Heutz, M.C. Wright, Emerging risk from "environmentally-friendly" solvents: Interaction of methylimidazolium ionic liquids with the mitochondrial electron transport chain is a key initiation event in their mammalian toxicity, Food Chem. Technol. 145 (2020).
[45] C. Velez, O. Acevedo, Simulation of deep eutectic solvents: Progress to promises, WIRESs Comput. Mol. Sci. 12 (2022) e1598.
[46] D. Tolmachev, N. Lukasheva, R. Ramazanov, V. Nazarychev, N. Borzdun, I. Volgin, M. Andreeva, A. Glova, S. Melnikova, A. Dobrovskiy, S.A. Silber, S. Larin, R.M. de Souza, M.C.C. Ribeiro, S. Lyulin, M. Karttunen, Computer simulations of deep eutectic solvents: challenges, solutions, and perspectives, Int. J. Mol. Sci. 23 (2022) 645.
[47] P. Kumari, V.V.S. Pillai, A. Benedetto, Mechanisms of action of ionic liquids on living cells: the state of the art, Biophys. Rev. 12 (2020) 1187–1215.
[48] A.S.L. Gouveia, L.C. Tome, I.M. Marrucho, Density, viscosity, and refractive index of ionic liquid mixtures containing cyano and amino acid-based anions, J. Chem. Eng. Data 61 (2016) 83.
[49] R. Alcalde, G. García, M. Atilhan, S. Aparicio, Systematic study on the viscosity of ionic liquids: measurement and prediction, Ind. Eng. Chem. Res. 54 (2015) 10918–10924.
[50] S.G. Balasubramani, G.P. Chen, S. Coriani, M. Diedenhofen, M.S. Frank, Y.J. Franzke, F. Furche, R. Grotjahn, M.E. Harding, C. Hättig, A.H.B. Helmich-Paris, et al., J. Chem. Phys. 152 (2020).
[51] S. Grimme, J. Antony, H. Krieg, A consistent and accurate ab initio parametrization of density functional dispersion correction (DFT-D) for the 94 elements H-Pu, J. Chem. Phys. 132 (2010).
[52] S. Simon, M. Duran, J. Dannenberg, How does basis set superposition error change the potential surfaces for hydrogen-bonded dimers?, J Chem. Phys. 105 (1996) 11024.
[53] R.F.W. Bader, Atoms in molecules, Acc. Chem. Res. 18 (1985) 9–15.
[54] L.u. Tian, F., Chen, Multiwfn: A multifunctional wavefunction analyzer, J. Comput. Chem. 33 (2012) 580–592.
[55] E.R. Johnson, S. Keinan, P. Mori-Sanchez, J. Contreras-García, A.J. Cohen, W. Yang, Revealing Noncovalent Interactions, J. Am. Chem. Soc. 132 (2010) 6498–6506.
[56] F. Fuster, B. Silvi, Theor. Does the topological approach characterize the hydrogen bond? Chem. Acc. 104 (2000) 13-21.
[57] BIOVIA COSMOtherm, Release 2021; Dassault Systèmes. http://www.3ds.com.
[58] A.P. Lyubartsev, A. Laaksonen, MDynaMix - A scalable portable parallel MD simulation package for arbitrary molecular mixtures, Comput. Phys. Commun 128 (2000) 565–589.
[59] P. Ren, J.W. Ponder, A. Grossfield, Ion Solvation Thermodynamics from Simulation with a Polarizable Force Field, J. Am. Chem. Soc. 125 (2003) 15671–15682.
[60] L. Martínez, R. Andrade, E.G. Birgin, J.M. Martínez, PACKMOL: a package for building initial configurations for molecular dynamics simulations, J. Comput. Chem. 30 (2009) 2157–2164.
[61] W.G. Hoover, Canonical dynamics: Equilibrium phase-space distributions, Phys. Rev. A 31 (1985) 1695–1697.
[62] U.L. Essmann, M.L. Perera, T. Berkowitz, H. Darden, H. Lee, L.G. Pedersen, J. Chem. Phys. 103 (1995) 8577.
[63] M. Brehm, B. Kirchner, TRAVIS - A free analyzer and visualizer for Monte Carlo and Molecular Dynamics trajectories, J. Chem. Inf. Model. 51 (2011) 2007–2023.
[64] W. Humphrey, A. Dalke, K. Schulten, VMD—Visual Molecular Dynamics, J. Molec. Graphics 14 (1996) 33–38.
[65] E. Mullins, R. Oldland, Y.A. Liu, S. Wang, S.I. Sandler, C.C. Chen, M. Zwolak, K.C. Seavey, Sigma-profile database for using COSMO-based thermodynamic methods, Ind. Eng. Chem. Res. 45 (2006) 4389–4415.
[66] P. López-Porfiri, J.F. Brennecke, M. González-Miquel, Excess enthalpies of deep eutectic solvents (DES) composed of quaternary ammonium salts and glycerol or ethylene glycol, J. Chem. Eng. Data 61 (2016) 4245–4251.
[67] G. Teizeira, D.O. Abranches, L.P. Silva, S.M. Vilas-Boa, S.P. Pinho, A.I.M.C.L. Ferreira, L.M.N.B.F. Santos, O. Ferreira, J.A.P. Coutinho, Liquefying flavonoids with terpenoids through deep eutectic solvents, Molecules 27 (2022) 2649.
[68] Y. Chen, W. Chen, L. Fu, Y. Yang, Y. Wang, X. Hu, F. Wang, T. Mu, Surface tension of 50 deep eutectic solvents: effect of hydrophobic doors, hydrogen bonding, acceptors, other solvents and temperature, Ind. Eng. Chem. Res. 58 (2019) 12741–12750.
[69] H.S. Salesi, O.A. Moultos, T.J.H. Vlugt, Interfacial properties of hydrophobic deep eutectic solvents with water, J. Phys. Chem. B 125 (2021) 12303–12314.
[70] C. Ma, A. Laaksonen, C. Liu, X. Lu, X. Ji, The peculiar effect of water on ionic liquids and deep eutectic solvents, Chem. Soc. Rev. 47 (2018) 8685–8720.
[71] S. Rozas, C. Benito, R. Alcalde, M. Atilhan, S. Aparicio, Insights on the water effect on deep eutectic solvents properties and structuring: The archetypical case of choline chloride + ethylene glycol, J. Mol. Liq. 344 (2021).
[72] H. Kivela, M. Slomaki, P. Vainikka, E. Makila, F. Poletti, S. Ruggeri, F. Terzi, J. Lukkari, Effect of water on hydrophobic deep eutectic solvent, J. Phys. Chem. B 126 (2022) 513–527.
[73] T. Lemaoui, A.S. Darwish, A. Attoui, F.A. Hatab, N. Hammoudi, Y. Benguerba, L.F. Vega, I.M. Alnashef, Predicting the density and viscosity of hydrophobic eutectic solvents: towards the development of sustainable solvents, Green Chem. 22 (2020) 8511–8530.
[74] D.J.G.P. van Osch, C.H.J.T. Dietz, S.E.E. Warrag, M.C. Kroon, The curious case of hydrophobic deep eutectic solvents: a story on the discovery, design and applications, ACS Sustainable Chem. Eng. 8 (2020) 10591–10612.

[75] A. Lucia, E. Zerba, H. Masuh, Knockdown and larvicidal activity of six monoterpenes against Aedes aegypti (Diptera: Culicidae) and their structure-activity relationships, Parasitol. Res. 112 (2013) 4267–4272.
[76] J. Sangster, Octanol-water partition coefficients of simple organic compounds, J. Phys. Chem. Ref. Data 18 (1989) 1111.
[77] F. Chemat, H. Anjum, A. Shariff, P. Kumar, T. Murugesan, Thermal and physical properties of (Choline chloride + urea + l-arginine) deep eutectic solvents, J. Mol. Liq. 218 (2016) 301–308.
[78] S. Aparicio, R. Alcalde, B. García, J.M. Leal, High-Pressure study of the methylsulfate and tosylate imidazolium ionic liquids, J. Phys. Chem. B 113 (2009) 5593–5606.
[79] H. Qin, Z. Song, H. Cheng, L. Deng, Z. Qi, Physical absorption of carbon dioxide in imidazole-PTSA based deep eutectic solvents, J. Mol. Liq. 326 (2021).
[80] J.Z. Zhang, X.M. Lu, J.S. Gui, W.G. Guo, A new theory for ionic liquids—the Interstice Model. Part 1. The density and surface tension of ionic liquid EMISE, Green Chem. 6 (2004) 541–543.
[81] A. Hofmann, M. Migeot, L. Arens, T. Hanemann, Investigation of Ternary Mixtures Containing 1-Ethyl-3-methylimidazolium Bis (trifluoromethanesulfonyl)azanide, Ethylene Carbonate and Lithium Bis (trifluoromethanesulfonyl)azanide, Int. J. Mol. Sci. 17 (2016) 670.
[82] S.S. Hossain, A. Samanta, Solute rotation and translation dynamics in an ionic deep eutectic solvent based on choline chloride, J. Phys. Chem. B 121 (2017) 10556–10565.
[83] H. Schulz, G.Ozkan, M. Baranska, H. Krüger, m. Ozcan, Characterisation of essential oil plants from Turkey by IR and Raman spectroscopy, Vibrational Spect. 39 (2005) 249-256.
[84] M. Baranska, H. Schulz, H. Krüger, R. Quilitzsch, Chemotaxonomy of aromatic plants of the genus Origanum via vibrational spectroscopy, Anal. Bioanal. Chem. 381 (2005) 1241–1247.
[85] M. Baranska, H. Schulz, S. Reitzenstein, U. Uhlemann, M.A. Strehle, h. Krüger, R. Quilitzsch, W. Foley, Vibrational spectroscopic studies to acquire a quality control method of Eucalyptus essential oils, Biopolymers 78 (2005) 237-248.
[86] S.D. Fried, S. Bagchi, S.G. Bozer, Measuring Electrostatic Fields in Both Hydrogen-Bonding and Non-Hydrogen-Bonding Environments Using Carbonyl Vibrational Probes, J. Am. Chem. Soc. 135 (2013) 11181–11192.
[87] M. Saggu, J. Liu, A. Patel, Identification of Subvisible Particles in Biopharmaceutical Formulations Using Raman Spectroscopy Provides Insight into Polysorbate 20 Degradation Pathway, Pharma Res. 32 (2015) 2877–2888.
[88] H. Kivela, M. Solomäki, P. Vainikka, E. Mäkila, F. Poletti, S. Ruggeri, F. Terzi, J. Lukkari, Effect of Water on a Hydrophobic Deep Eutectic Solvent, J. Phys. Chem. B 126 (2022) 513–527.
[89] H. Zhang, Z. Chen, T. Li, N. Chen, W. Xu, S. Liu, Surface-enhanced Raman scattering spectra revealing the inter-cultivar diferences for Chinese ornamental Flos Chrysanthemum: a new promising method for plant taxonomy, Plant Methods 13 (2017) 92.
[90] C. Fan, T. Sebbah, X. Cao, A theoretical study on terpene-based natural deep eutectic solvent: relationship between viscosity and hydrogen-bonding interactions, Global Challen. 5 (2021) 2000103.
[91] A. Gutiérrez, L. Zamora, C. Benito, M. Atilhan, S. Aparicio, Insights on novel type V deep eutectic solvents based on levulinic acid, J. Chem. Phys. 156 (2022).
[92] M. Santra, D. Kunzru, D. Rabari, A stability analysis of choline chloride: urea deep eutectic solvent using density functional theory, Comput. Theoret. Chem. 1217 (2022).
[93] U. Koch, P.L.P. Popelier, Characterization of C-H-O hydrogen bonds on the basis of the charge density, J. Phys. Chem. 99 (1995) 9747–9754.
[94] M.B. Wenny, N. Molinari, A.H. Slavney, S. Thapa, B. Lee, B. Kozinsky, J.A. Mason, Understanding relationships between free volume and oxygen absorption in ionic liquids, J. Phys. Chem. B 126 (2022) 1268–1274.
[95] W. Beicherl, Y. Yu, G. Dlubek, R. Krauser-Rehberg, J. Piontek, D. Pfefferkom, S. Bulut, D. Bejan, C. Friedrich, I. Krossing, Free volume in ionic liquids: a connection of experimentally accessible observables from PALS and PVT experiments with the molecular structure from XRD data, Phys. Chem. Chem. Phys. 15 (2013) 8821–8830.
[96] N.J. Brooks, F. Castiglione, C.M. Doherty, A. Dolan, A.J. Hill, P.A. Hunt, R.P. Matthews, M. Mauri, A. Mele, R. Simonutti, I.J. villar-García, C.C. Weber, T. Welton, Linking the structures, free volumes, and properties of ionic liquid mixtures, Chem. Sci. 8 (2017) 6359-6374.
[97] I. Delso, C. Lafuente, J. Muñoz-Embid, M. Artal, NMR study of choline chloride-based deep eutectic solvents, J. Mol. Liq. 290 (2019).
[98] S.B. Pour, J.J. Sardroodi, A.R. Ebrahimzadeh, The study of structure and interactions of glucose-based natural deep eutectic solvents by molecular dynamics simulation, J. Mol. Liq. 334 (2021).
[99] T. Köddermann, R. Ludwig, D. Paschek, On the Validity of Stokes-Einstein and Stokes–Einstein–Debye Relations in Ionic Liquids and Ionic-Liquid Mixtures, ChemPhysChem 9 (2008) 1851–1858.